COMMUNICATIONS IN COMPUTATIONAL PHYSICS
Vol. **6**, No. 1, pp. 131-161

Commun. Comput. Phys.
July 2009

Laplace-Transform Finite Element Solution of Nonlocal and Localized Stochastic Moment Equations of Transport

Eric Morales-Casique and Shlomo P. Neuman*

Department of Hydrology and Water Resources, University of Arizona, Tucson, Arizona 85721, USA.

Received 26 November 2007; Accepted (in revised version) 25 October 2008

Available online 18 November 2008

Abstract. Morales-Casique et al. (Adv. Water Res., 29 (2006), pp. 1238-1255) developed exact first and second nonlocal moment equations for advective-dispersive transport in finite, randomly heterogeneous geologic media. The velocity and concentration in these equations are generally nonstationary due to trends in heterogeneity, conditioning on site data and the influence of forcing terms. Morales-Casique et al. (Adv. Water Res., 29 (2006), pp. 1399-1418) solved the Laplace transformed versions of these equations recursively to second order in the standard deviation σ_Y of (natural) log hydraulic conductivity, and iteratively to higher-order, by finite elements followed by numerical inversion of the Laplace transform. They did the same for a space-localized version of the mean transport equation. Here we recount briefly their theory and algorithms; compare the numerical performance of the Laplace-transform finite element scheme with that of a high-accuracy ULTIMATE-QUICKEST algorithm coupled with an alternating split operator approach; and review some computational results due to Morales-Casique et al. (Adv. Water Res., 29 (2006), pp. 1399-1418) to shed light on the accuracy and computational efficiency of their recursive and iterative solutions in comparison to conditional Monte Carlo simulations in two spatial dimensions.

AMS subject classifications: 65Z05, 65Z05, 68U20, 76S05

Key words: Geologic media, porous media, random heterogeneity, conditioning, stochastic transport, moment equations, nonlocality, localization, Laplace transform, finite elements, ultimate-quickest.

1 Introduction

It has become increasingly common to describe the spatial variability of geologic medium properties geostatistically and to analyze subsurface fluid flow and solute transport in

*Corresponding author. *Email addresses:* emorales@hwr.arizona.edu (E. Morales-Casique), neuman@hwr.arizona.edu (S. P. Neuman)

such media stochastically [11,44,55]. The most common and straightforward method of stochastic analysis is computational Monte Carlo simulation that produces a large number of equally likely results. These results are summarized statistically in terms of their sample averages, second (variance-covariance) or higher moments, or probability distributions. Results that honor measured values of medium properties and/or state variable are said to be conditioned on these data. One thus obtains (among others) conditional mean flow and transport variables that constitute optimum unbiased predictors of these random quantities, and conditional second moments that provide a measure of the associated prediction errors. An alternative is to compute these statistics directly on the basis of corresponding conditional moment equations. Commonly, the moment equations are derived *a priori* in an approximate manner which renders them local in space-time. We focus instead on exact forms of these equations, which are generally nonlocal in space-time, and their subsequent solution by approximation.

Exact space-time nonlocal first and second conditional moment equations have been developed for steady state [40,41] and transient [48–50] flow in bounded saturated media as well as advective [23,39] and advective-dispersive [56] transport in infinite domains; related but somewhat different unconditional formulations of nonlocal transport in such domains are found in [10,15,30]. We concentrate here on exact first and second nonlocal moment equations for advective-dispersive transport in bounded media developed recently by Morales-Casique et al. [37]. Morales-Casique et al. [38] solved Laplace transformed versions of these equations recursively to second order in the standard deviation σ_Y of (natural) log hydraulic conductivity, and iteratively to higher-order, by finite elements followed by numerical inversion of the Laplace transform. They did the same for a space-localized version of the mean transport equation. Following a summary of their theory and algorithmic approach, we compare below the numerical performance of the Laplace-transform finite element scheme with that of a high-accuracy ULTIMATE-QUICKEST algorithm coupled with an alternating split operator approach. We then review some computational results due to Morales-Casique et al. [38] to shed light on the accuracy and computational efficiency of their recursive and iterative solutions in comparison to conditional and unconditional Monte Carlo simulations in two spatial dimensions.

2 Exact conditional moment equations for bounded media

Morales-Casique et al. [37] express advective-dispersive solute mass flux at some local support scale ω, centered about point $\mathbf{x}$ in a Cartesian coordinate system, as

$$\mathbf{J}(\mathbf{x},t)=\mathbf{v}(\mathbf{x},t)c(\mathbf{x},t)-\mathbf{D}_d\nabla c(\mathbf{x},t), \tag{2.1}$$

where c is concentration, $\mathbf{v}$ is velocity, $\mathbf{D}_d$ is a constant local dispersion tensor and t is time. The velocity is given by Darcy's law

$$\mathbf{v}(\mathbf{x},t)=-K(\mathbf{x})\nabla h(\mathbf{x},t)/\phi,$$

where $K(\mathbf{x})$ is a random hydraulic conductivity field, $h(\mathbf{x},t)$ is hydraulic head and ϕ is a constant porosity. It satisfies a stochastic flow equation

$$\nabla\cdot\mathbf{v}(\mathbf{x},t)=f(\mathbf{x},t)$$

subject to random initial and boundary conditions where $f(\mathbf{x},t)$ is a random fluid source (and/or accumulation term involving $\partial h/\partial t$) normalized by ϕ. Lead multivariate statistics of log hydraulic conductivity $Y(\mathbf{x})=\ln K(\mathbf{x})$ are inferred geostatistically from measured values of $K(\mathbf{x})$, rendering it conditional on these data and thus (generally) non-stationary [11, 44]. Lead joint statistics of $\mathbf{v}$ and f are obtained by solving the stochastic flow equation subject to appropriate (generally random) initial and boundary conditions, conditioned on measurements of $K(\mathbf{x})$ and/or $h(\mathbf{x},t)$ and $\mathbf{v}(\mathbf{x},t)$ by forward and/or inverse solutions using Monte Carlo simulation or the solution of corresponding recursive conditional moments equations [23, 24, 28, 54].

The concentration of a non-reactive solute in a domain Ω bounded by Γ is taken to be governed locally by the advection-dispersion equation

$$\frac{\partial c(\mathbf{x},t)}{\partial t}+\nabla\cdot\mathbf{J}(\mathbf{x},t)=g(\mathbf{x},t),\qquad \mathbf{x}\in\Omega \tag{2.2}$$

subject to initial and boundary conditions

$$c(\mathbf{x},0)=C_0(\mathbf{x}),\qquad \mathbf{x}\in\Omega, \tag{2.3}$$
$$c(\mathbf{x},t)=C_D(\mathbf{x},t),\qquad \mathbf{x}\in\Gamma_1, \tag{2.4}$$
$$-\mathbf{D}_d\nabla c(\mathbf{x},t)\cdot\mathbf{n}(\mathbf{x})=W(\mathbf{x},t),\qquad \mathbf{x}\in\Gamma_2, \tag{2.5}$$
$$[\mathbf{v}(\mathbf{x},t)c(\mathbf{x},t)-\mathbf{D}_d\nabla c(\mathbf{x},t)]\cdot\mathbf{n}(\mathbf{x})=P(\mathbf{x},t),\quad \mathbf{x}\in\Gamma_3, \tag{2.6}$$

where g is a random source of solute, C_D is a random concentration prescribed on boundary segment Γ_1, W is a random dispersive flux prescribed normal to boundary segment Γ_2, P is a random advective-dispersive flux prescribed on boundary segment Γ_3, and $\mathbf{n}$ is an outward unit normal to any segment of Γ. Though theory does not require it, all forcing terms g, C_0, C_D, W, P are taken to be prescribed in a manner that renders them statistically independent of $\mathbf{v}$ and each other. All random functions $a(\mathbf{x},t)$ are decomposed as

$$a(\mathbf{x},t)=\langle a(\mathbf{x},t)\rangle_c+a'(\mathbf{x},t),\quad \langle a'(\mathbf{x},t)\rangle_c\equiv 0,$$

where $\langle\ \rangle_c$ designates ensemble mean conditioned on measurements (as implied by the subscript; for simplicity and without loss of generality, forcing terms remain unconditional) and primed quantities are zero-mean random fluctuations about the mean. The former can be viewed as unbiased predictors of their random counterparts, and the latter as the associated prediction errors. Morales-Casique et al. [37] show that conditional mean transport is governed exactly by

$$\frac{\partial}{\partial t}\langle c(\mathbf{x},t)\rangle_c+\nabla\cdot\langle\mathbf{J}(\mathbf{x},t)\rangle_c=\langle g(\mathbf{x},t)\rangle,\qquad \mathbf{x}\in\Omega \tag{2.7}$$

subject to

$$\langle c(\mathbf{x},0)\rangle_c = \langle C_0(\mathbf{x})\rangle, \qquad \mathbf{x}\in\Omega, \tag{2.8}$$

$$\langle c(\mathbf{x},t)\rangle_c = \langle C_D(\mathbf{x},t)\rangle, \qquad \mathbf{x}\in\Gamma_1, \tag{2.9}$$

$$-\mathbf{D}_d\nabla\langle c(\mathbf{x},t)\rangle_c\cdot\mathbf{n}(\mathbf{x}) = \langle W(\mathbf{x},t)\rangle, \qquad \mathbf{x}\in\Gamma_2, \tag{2.10}$$

$$[\langle\mathbf{v}(\mathbf{x},t)\rangle_c\langle c(\mathbf{x},t)\rangle_c - \mathbf{D}_d\nabla\langle c(\mathbf{x},t)\rangle_c + \mathbf{Q}_c(\mathbf{x},t)]\cdot\mathbf{n}(\mathbf{x}) = \langle P(\mathbf{x},t)\rangle, \quad \mathbf{x}\in\Gamma_3, \tag{2.11}$$

where

$$\langle\mathbf{J}(\mathbf{x},t)\rangle_c = \langle\mathbf{v}(\mathbf{x},t)\rangle_c\langle c(\mathbf{x},t)\rangle_c - \mathbf{D}_d\nabla\langle c(\mathbf{x},t)\rangle_c + \mathbf{Q}_c(\mathbf{x},t), \tag{2.12}$$

$$\begin{aligned}\mathbf{Q}_c(\mathbf{x},t) = &\int_\Omega\int_0^t \boldsymbol{\alpha}_c(\mathbf{x},t,\mathbf{y},\tau)\nabla_y\cdot\mathbf{Q}_c(\mathbf{y},\tau)d\tau d\mathbf{y} - \int_\Omega\int_0^t \boldsymbol{\beta}_c(\mathbf{x},t,\mathbf{y},\tau)\nabla_y\langle c(\mathbf{y},\tau)\rangle_c d\tau d\mathbf{y}\\ &- \int_\Omega\int_0^t \gamma_c(\mathbf{x},t,\mathbf{y},\tau)\langle c(\mathbf{y},\tau)\rangle_c d\tau d\mathbf{y} - \int_{\Gamma_3}\int_0^t \boldsymbol{\alpha}_c(\mathbf{x},t,\mathbf{y},\tau)\mathbf{Q}_c^T(\mathbf{y},\tau)\mathbf{n}(\mathbf{y})d\tau d\mathbf{y}\\ &+ \int_{\Gamma_3}\int_0^t \boldsymbol{\beta}_c(\mathbf{x},t,\mathbf{y},\tau)\langle c(\mathbf{y},\tau)\rangle_c\mathbf{n}(\mathbf{y})d\tau d\mathbf{y},\end{aligned} \tag{2.13}$$

and

$$\begin{aligned}\boldsymbol{\alpha}_c(\mathbf{x},t,\mathbf{y},\tau) &= \left\langle G(\mathbf{x},t|\mathbf{y},\tau)\mathbf{v}'(\mathbf{x},t)\right\rangle_c,\\ \boldsymbol{\beta}_c(\mathbf{x},t,\mathbf{y},\tau) &= \left\langle G(\mathbf{x},t|\mathbf{y},\tau)\mathbf{v}'(\mathbf{x},t)\mathbf{v}'^T(\mathbf{y},\tau)\right\rangle_c,\\ \gamma_c(\mathbf{x},t,\mathbf{y},\tau) &= \langle G(\mathbf{x},t|\mathbf{y},\tau)\mathbf{v}'(\mathbf{x},t)f'(\mathbf{y},\tau)\rangle_c.\end{aligned}$$

The random Green's function $G(\mathbf{x},t|\mathbf{y},\tau)$ satisfies a stochastic advection-dispersion equation subject to homogenous initial and boundary conditions. Morales-Casique et al. [37] present corresponding equations satisfied exactly by the conditional covariance

$$C_{cc}(\mathbf{x},t,\mathbf{z},s) = \langle c'(\mathbf{x},t)c'(\mathbf{z},s)\rangle_c$$

of concentration and the conditional covariance $\langle\mathbf{J}'(\mathbf{x},t)\mathbf{J}'^T(\mathbf{z},s)\rangle_c$ of solute flux.

3 Recursive and iterative Laplace-transform finite element algorithms (FELT)

Though the above conditional moment equations are exact, they cannot be evaluated without a closure approximation. For steady state flow Morales-Casique et al. [37] derive recursive approximations in Laplace space by expanding all ensemble moments to i^{th} order in a small parameter, σ_Y, representing the standard deviation of

$$Y'(\mathbf{x}) = Y(\mathbf{x}) - \langle Y(\mathbf{x})\rangle_c.$$

They define a deterministic differential operator

$$\hat{L}^{(0)} = \lambda + \nabla \cdot [\langle \mathbf{v}(\mathbf{x}) \rangle_c^{(0)} - \mathbf{D}_d \nabla],$$

where tilde designates Laplace transformed quantities and the superscript indicates order zero in σ_Y. They show that, to zero order, $\langle \hat{c}(\mathbf{x},\lambda) \rangle_c$ satisfies the boundary-value problem

$$\hat{L}^{(0)} \langle \hat{c}(\mathbf{x},\lambda) \rangle_c^{(0)} = \langle \hat{g}(\mathbf{x},\lambda) \rangle + \langle C_0(\mathbf{x}) \rangle, \qquad \mathbf{x} \in \Omega, \tag{3.1}$$

$$\langle \hat{c}(\mathbf{x},\lambda) \rangle_c^{(0)} = \langle \hat{C}_D(\mathbf{x},\lambda) \rangle, \qquad \mathbf{x} \in \Gamma_1, \tag{3.2}$$

$$-\mathbf{D}_d \nabla \langle \hat{c}(\mathbf{x},\lambda) \rangle_c^{(0)} \cdot \mathbf{n}(\mathbf{x}) = \langle \hat{W}(\mathbf{x},\lambda) \rangle, \qquad \mathbf{x} \in \Gamma_2, \tag{3.3}$$

$$\left[\langle \mathbf{v}(\mathbf{x}) \rangle_c^{(0)} \langle \hat{c}(\mathbf{x},\lambda) \rangle_c^{(0)} - \mathbf{D}_d \nabla \langle \hat{c}(\mathbf{x},\lambda) \rangle_c^{(0)} \right] \cdot \mathbf{n}(\mathbf{x}) = \langle \hat{P}(\mathbf{x},\lambda) \rangle, \quad \mathbf{x} \in \Gamma_3, \tag{3.4}$$

and to second order the boundary-value problem

$$\hat{L}^{(0)} \langle \hat{c}(\mathbf{x},\lambda) \rangle_c^{(2)} = -\langle \mathbf{v}(\mathbf{x}) \rangle_c^{(2)} \cdot \nabla \langle \hat{c}(\mathbf{x},\lambda) \rangle_c^{(0)} - \nabla \cdot \hat{\mathbf{Q}}_c^{(2)}(\mathbf{x},\lambda), \qquad \mathbf{x} \in \Omega, \tag{3.5}$$

$$\langle \hat{c}(\mathbf{x},\lambda) \rangle_c^{(2)} = 0, \qquad \mathbf{x} \in \Gamma_1, \tag{3.6}$$

$$-\mathbf{D}_d \nabla \langle \hat{c}(\mathbf{x},\lambda) \rangle_c^{(2)} \cdot \mathbf{n}(\mathbf{x}) = 0, \qquad \mathbf{x} \in \Gamma_2, \tag{3.7}$$

$$\begin{aligned} &\left[\langle \mathbf{v}(\mathbf{x}) \rangle_c^{(0)} \langle \hat{c}(\mathbf{x},\lambda) \rangle_c^{(2)} - \mathbf{D}_d \nabla \langle \hat{c}(\mathbf{x},\lambda) \rangle_c^{(2)} \right] \cdot \mathbf{n}(\mathbf{x}) \\ &\quad = -\left[\langle \mathbf{v}(\mathbf{x}) \rangle_c^{(2)} \langle \hat{c}(\mathbf{x},\lambda) \rangle_c^{(0)} + \hat{\mathbf{Q}}_c^{(2)}(\mathbf{x},\lambda) \right] \cdot \mathbf{n}(\mathbf{x}), \qquad \mathbf{x} \in \Gamma_3. \end{aligned} \tag{3.8}$$

The complete second-order approximation is given by

$$\langle \hat{c} \rangle_c^{[2]} = \langle \hat{c} \rangle_c^{(0)} + \langle \hat{c} \rangle_c^{(2)}.$$

The authors provide corresponding second order equations for the conditional covariance of concentration prediction errors, $\hat{\mathbf{Q}}_c^{(2)}$ and solute mass flux.

Eqs. (3.1) and (3.5) are Laplace-transformed equivalents of a standard advection-dispersion problem but with nonstandard forcing terms and variables (including parameters) that constitute deterministic estimators of their random counterparts. Eqs. (3.1)-(3.8) can therefore be solved using existing numerical methods supplemented with routines to compute the forcing terms. Morales-Casique et al. [38] solve these recursive moment equations by Galerkin finite elements in a rectangular domain Ω subject to deterministic initial and boundary conditions, taking the velocity to be uniform in each element and the local dispersion-diffusion coefficient to be a constant deterministic scalar, D_d. They invert the results back into the time domain using a numerical algorithm due to Crump [9] and De Hoog et al. [14]. The authors demonstrate that an improved solution is obtained upon adopting the iterative solution algorithm (Algorithm 3.1).

The results form an incomplete third order approximation, as indicated by the superscript $(2+)$ in that the algorithm excludes the third-moment $\nabla_z \cdot \langle \hat{c}' \mathbf{v}' v_i' \rangle_c$.

Algorithm 3.1:

a) Solve (3.1)-(3.4) for $\langle\hat{c}\rangle_c^{(0)}$ and set $\langle\hat{c}\rangle_c^{old}=\langle\hat{c}\rangle_c^{(0)}$.

b) Evaluate $\hat{Q}_{ci}^{(2+)}$ using $\langle\hat{c}\rangle_c^{old}$ instead of $\langle\hat{c}\rangle_c^{(0)}$.

c) Solve (3.5)-(3.8) for $\langle\hat{c}\rangle_c^{(2+)}$ using $\langle\hat{c}\rangle_c^{(0)}$ and $\hat{\mathbf{Q}}_c^{(2+)}$.

d) Compute $\langle\hat{c}\rangle_c^{new}=\langle\hat{c}\rangle_c^{(0)}+\langle\hat{c}\rangle_c^{(2+)}$.

e) If $\left|\langle\hat{c}\rangle_c^{new}-\langle\hat{c}\rangle_c^{old}\right|$ exceeds a predetermined tolerance, set $\langle\hat{c}\rangle_c^{old}=\langle\hat{c}\rangle_c^{new}$ and go back to step b.

f) Evaluate $\hat{C}_{cc}^{(2+)}$ using $\langle\hat{c}\rangle_c^{new}$ and $\hat{\mathbf{Q}}_c^{(2+)}$ instead of $\langle\hat{c}\rangle_c^{(0)}$ and $\hat{\mathbf{Q}}_c^{(2)}$.

Morales-Casique et al. [38] also examine a space-localized finite element solution (designated by the superscript L) with dispersive flux

$$\hat{Q}_{ci}^{L}(\mathbf{x},\lambda)=\hat{\mathbf{D}}^{(2)}(\mathbf{x},\lambda)\nabla\left\langle c'(\mathbf{x},\lambda)\right\rangle_c^L,$$

which becomes a time-convolution integral in the time domain.

4 Comparison of FELT with another high-accuracy scheme

We compare below the Laplace transform finite element algorithm (FELT) used by Morales-Casique et al. [37, 38] with another high-accuracy approach, motivated by the following considerations. Solving the stochastic transport problem by numerical Monte Carlo simulation requires a computational grid that is fine enough to resolve ω-scale random velocity fluctuations. As ω-scale dispersivities are relatively small, each Monte Carlo run tends to be dominated by advection. Each conditional Monte Carlo run produces a space-time realization of ω-scale velocity, solute concentration and mass flux which, upon averaging over numerous realizations, yields sample statistical moments of these quantities. An alternative method of solving stochastic transport problems is to compute ensemble moments of these quantities directly by solving a system of ensemble moment equations such as those mentioned earlier. The corresponding zero-order moment equations entail only a local, ω-scale dispersion term that render them advection-dominated in many cases of interest. Second-order moment equations include a macrodispersion term that is initially zero but grows with solute residence time toward values that may become large in comparison to local dispersion [56]. Hence second-order moment equations are advection dominated at early time while tending to be less so at later times. It follows that solving stochastic transport equations, by whatever method, is subject to the usual numerical difficulties associated with advection-dominated problems. In particular, standard upstream numerical schemes tend to exhibit artificial smearing of sharp concentration fronts and centered schemes tend to generate spurious oscillations that may manifest themselves as concentration overshoot, undershoot and clipping

of peaks. The first phenomenon results from truncation errors of insufficiently high order, the second from variable propagation speeds of short-wave components in a Fourier representation of the numerical solution [21].

Among modern computational approaches designed to deal with some of these problems we count the Eulerian-Lagrangian localized adjoint method (ELLAM) [5, 29], the streamline method [2, 12], total-variation-diminishing (TVD) methods [35], essentially (ENO) and uniformly (UNO) nonoscillatory methods [26, 27], and Laplace-transform finite elements (FELT) [42,46,53] in which a finite element solution of Laplace-transformed transport equations is transformed back into the time domain using numerical inversion. A summary of some of these and other approaches was published by Ewing and Wang [18]. Al-Lawatia et al. [1] compared Runge-Kutta characteristic ELLAM methods with Crank-Nicholson finite element (Galerkin, Quadratic and Cubic Petrov-Galerkin), streamline diffusion, continuous and discontinuous Galerkin and two high-accuracy finite volume schemes (monotone upstream-centered scheme for conservation laws MUSCL [51, 52] and MINMOD [35]) for one-dimensional advection-dispersion. They found ELLAM to be more accurate and efficient than other schemes: whereas second-order TVD schemes generated monotonous profiles with some numerical dispersion, all other schemes but ELLAM developed spurious oscillations, all requiring finer space-time grids and much more computer time than ELLAM. However, the authors noted that ELLAM might not work well in the case of multidimensional problems with spatially varying velocity.

Farthing and Miller [20] conducted a thorough review and comparison of leading high-accuracy finite-volume schemes. Among 14 such schemes (including MUSCL and MINMOD) they found two higher-order TVD schemes, ULTIMATE-QUICKEST [33] and the piecewise parabolic method PPM [6], to perform well on their test problems and to be generally more efficient than the best lower order TVD method (MUSCL) and the three uniformly nonoscillatory (UNO) and essentially nonoscillatory (ENO) schemes they had evaluated. In particular ULTIMATE-QUICKEST seemed to offer the most attractive balance between accuracy and computational efficiency. The scheme was recently incorporated in the popular groundwater transport code MT3DMS [57].

Stochastic moment equations include temporal convolution integrals which FELT reduces to simple products in the Laplace-transformed domain. In addition, FELT provides time-continuous solutions that are free of restrictions on the Courant number, mutually independent and so amenable to parallel computation, and independent of solutions at previous time values. On the other hand FELT is limited to linear transport equations associated with time-independent velocity fields, may suffer from oscillations (Gibbs phenomenon) near discontinuities due to truncation errors, and may be less efficient than time marching schemes when a solution is required at many time values. Based on these considerations we decided to compare FELT with ULTIMATE-QUICKEST identified by Farthing and Miller [20] as one of the best performing higher-order TVD schemes. Our numerical examples include a composite 1-D concentration profile in a uniform velocity field, 1-D transport due to an instantaneous point source in such a field, 2-D transport in a

randomly varying velocity field arising from random medium heterogeneity, and Monte Carlo simulated mean 2-D transport in mildly and strongly heterogeneous random media.

4.1 Background

Total variation diminishing (TVD) finite volume schemes

In one-dimension the advection equation can be approximated by the finite difference conservation form

$$c_i^{n+1} = c_i^n - \frac{\Delta t}{\Delta x}[F(c_{i+1/2}) - F(c_{i-1/2})], \tag{4.1}$$

where i is sequential node number, c_i^n is an approximation of the cell averaged concentration $\bar{c}_i^n = \frac{1}{\Delta x}\int_{x_{i-1/2}}^{x_{i+1/2}} c(x,t_n)dx$ at time t_n (time step n) in a cell bounded by $x_{i-1/2}$ and $x_{i+1/2}$, and $F(c_{i+1/2}) = \frac{1}{\Delta t}\int_{t_n}^{t_{n+1}} f(c_{i+1/2})dt$ is time-averaged advective solute flux $f(c_{i+1/2}) = v_{i+1/2}c_{i+1/2}$ at $x_{i+1/2}$. The total variation (TV) of c^n across the grid is defined as [35]

$$\mathrm{TV}(c^n) = \sum_{i=1}^{N-1} \left| c_{i+1}^n - c_i^n \right|, \tag{4.2}$$

where N is the number of nodes. A numerical scheme is said to be total-variation-diminishing or TVD if

$$\mathrm{TV}(c^{n+1}) \le \mathrm{TV}(c^n) \quad \text{for every } n.$$

Spurious oscillations bring about an increase in TV which may cause (4.2) to be violated. One way to suppress such oscillations is to enforce (4.2) by adding numerical diffusion to a higher-order scheme near sharp fronts using flux- or slope-limiters [35].

Early TVD methods such as the flux-corrected approach [4], Superbee limiter [43], MUSCL [52] and MINMOD [35] were second-order accurate. Current schemes such as that of Cox and Nishikawa [8], ULTIMATE-QUICKEST [33] and PPM [6] include modifications to improve accuracy in smooth regions. We focus below on the ULTIMATE-QUICKEST scheme.

ULTIMATE-QUICKEST scheme

Consider a monotonic one-dimensional concentration profile $c_{i-1}^n \le c_i^n \le c_{i+1}^n \le c_{i+2}^n$ advected by a positive spatially varying velocity $v > 0$. The conservation expression (4.1) now takes the form

$$c_i^{n+1} = c_i^n - \frac{\Delta t}{\Delta x}\left[v_{i+1/2}c_{i+1/2} - v_{i-1/2}c_{i-1/2}\right], \tag{4.3}$$

where $c_{1+1/2}$ is limited by $c_i^n \le c_{i+1/2} \le c_{i+1}^n$. Maintaining monotonicity requires

$$c_{i-1}^n \le c_i^{n+1} \le c_{i+1}^n.$$

By virtue of (4.3) and considering that $v_{i-1/2}>0$, the left inequality transforms into

$$v_{i+1/2}c_{i+1/2}\leq v_{i-1/2}c_{i-1/2}+\left(c_i^n-c_{i-1}^n\right)\Delta x/\Delta t,$$

which, for a worst-case estimate of $c_{i-1/2}^n$, yields

$$v_{i+1/2}c_{i+1/2}\leq v_{i-1/2}c_{i-1}+\frac{\Delta x}{\Delta t}\left(c_i^n-c_{i-1}^n\right). \tag{4.4}$$

Likewise, the right inequality in $c_i^n\leq c_{i+1/2}\leq c_{i+1}^n$ transforms into

$$v_{i-1/2}c_{i-1/2}\leq v_{i+1/2}c_{i+1/2}+\left(c_{i+1}^n-c_i^n\right)\Delta x/\Delta t.$$

Viewing $c_{i+1/2}$ as concentration at the left face of a cell centered about $i+1$ and adopting a worst-case estimate for $c_{i+3/2}$ yields

$$v_{i+1/2}c_{i+1/2}\leq v_{i+3/2}c_{i+1}+\frac{\Delta x}{\Delta t}\left(c_{i+2}^n-c_{i+1}^n\right),\qquad v_{i+3/2}>0. \tag{4.5}$$

For constant advective velocity (4.5) is replaced by $c_{i+1/2}\leq c_{i+1}^n$ in $c_i^n\leq c_{i+1/2}\leq c_{i+1}^n$. For local extrema one sets $c_{i+1/2}=c_i^n$. Inequalities (4.4) and (4.5) constitute the universal limiter ULTIMATE [33]. In practice, it needs to be applied only near sharp gradients where the constraints could be violated. Leonard [33] considered several high-order interpolation schemes to compute the cell-face values $c_{i+1/2}$ among which the simplest, yet sufficiently accurate, is the third order QUICKEST interpolator. The algorithm implemented in this work for a constant positive velocity is [33]:

Algorithm 4.1:

---

a) Compute $|DEL|=\left|c_{i+1}^n-c_i^n\right|$ and $|CURV|=\left|c_{i+1}^n-2c_i^n+c_{i-1}^n\right|$.

b) If $|CURV|\leq 0.6|DEL|$ use the unconstrained QUICKEST face value

$$c_{i+1/2}^{QUICK}=\frac{1}{2}\left(c_{i+1}^n+c_i^n\right)-\frac{Cr}{2}\left(c_{i+1}^n-c_i^n\right)-\frac{1}{6}\left(1-Cr^2\right)CURV,$$

where $Cr=v\Delta t/\Delta x$ is the Courant number.

c) If $|CURV|\geqslant|DEL|$ (local extrema) set $c_{i+1/2}=c_i^n$.

d) Otherwise use the ULTIMATE limiter to set $c_{i+1/2}^{ref}=c_{i-1}^n+\frac{1}{Cr}\left[c_i^n-c_{i-1}^n\right]$.

e) If $DEL>0$ (monotonic increasing) limit $c_{i+1/2}$ first by $c_{i+1/2}=\max\left(c_{i+1/2}^{QUICK},c_i^n\right)$ and then by $c_{i+1/2}=\min\left(c_{i+1/2},c_{i+1/2}^{ref},c_{i+1}^n\right)$.

f) If $DEL<0$ (monotonic decreasing) limit $c_{i+1/2}$ first by $c_{i+1/2}=\min\left(c_{i+1/2}^{QUICK},c_i^n\right)$ and then by $c_{i+1/2}=\max\left(c_{i+1/2},c_{i+1/2}^{ref},c_{i+1}^n\right)$.

The extension to two dimensions of the ULTIMATE-QUICKEST algorithm for advective transport is detailed in Leonard and Niknafs [34]; we employ this algorithm in our two-dimensional simulations as implemented in the code MT3DMS [57].

In applying the one- and two-dimensional algorithms to advective-dispersive transport we adopt an alternating split operator approach [36,45] as implemented by Farthing and Miller [20]:

a) Solve a pure dispersion problem using a Crank-Nicholson scheme over the first half of a time step $[t,t+\Delta t/2]$ with $c(x,t)$ as initial concentration.

b) Solve a pure advection problem over the entire time step $[t,t+\Delta t/2]$ with c from (a) as initial concentration.

c) Solve a pure dispersion problem using a Crank-Nicholson scheme over the second half of the time step $[t+\Delta t/2,t+\Delta t]$ with c from (b) as initial concentration.

FELT scheme

Applying the Laplace transform to the advection dispersion equation yields

$$\lambda\hat{c}(\mathbf{x},\lambda)+\nabla\cdot[\mathbf{v}(\mathbf{x})\hat{c}(\mathbf{x},\lambda)-\mathbf{D}_d\nabla\hat{c}(\mathbf{x},\lambda)]-\hat{g}(\mathbf{x},\lambda)-C_0(\mathbf{x})=0, \tag{4.6}$$

where λ is a complex parameter with $\mathrm{Re}(\lambda)>0$, $\hat{c}$ and $\hat{g}$ are Laplace transforms of c and g, respectively, and C_0 is initial concentration. In FELT (4.6) is solved by finite elements and the results are inverted numerically back into the time domain. As the finite element equations entail complex, generally nonsymmetric coefficient matrices, we presently solve them using the IMSL (`http://www.vni.com/products/imsl/`) *LU*-factorization subroutine DLSACB with iterative refinement for improved accuracy.

To obtain a solution in the time domain Sudicky [46] used the Crump inverse Laplace transform algorithm [9] due to its accuracy and reasonable performance near discontinuities. For a given point in space, the corresponding inverse is given by

$$c(\mathbf{x},t)=\frac{e^{\lambda_0 t}}{T}\left\{\frac{\hat{c}(\mathbf{x},\lambda_0)}{2}+\sum_{k=1}^{2M+1}\mathrm{Re}\left[\hat{c}(\mathbf{x},\lambda_k)e^{\left(i\frac{\pi k}{T}t\right)}\right]\right\}, \tag{4.7}$$

where the inverse Laplace transform is discretized using a trapezoidal rule with mesh size π/T and the Laplace parameter is expressed as $\lambda_k=\lambda_0+i\pi k/T$, $k=1,\cdots,2M+1$. Although the optimal selection of parameters is problem dependent, Crump recommended $\lambda_0=\mu-\ln(Er)/T$ where $T=0.8t_{max}$, t_{max} being the maximum time of interest, $\mu=0$, $10^{-2}\leq Er\leq 10^{-8}$, Er being a measure of accuracy, and the inverse is computed within the interval $0<t<2T$. To avoid instability at early time Gallo et al. [22] recommend setting $t>0.1t_{max}$. They also recommend limiting $M\leq 25$ to minimize roundoff errors; however, we found that in the presence of sharp gradients a more accurate solution is obtained by setting $M=30$.

Crump [9] employed a so-called epsilon algorithm to evaluate (4.7). de Hoog et al. [14] improved the rate of convergence by computing a diagonal Padé approximation to the

series in (4.7), known as the quotient-difference (*q-d*) algorithm. They proposed an additional accelerated convergence procedure that estimates the remainder of the continued fraction. The q-d algorithm leads to a significant improvement in accuracy and is highly efficient when inversion is required for many time values. This is the algorithm we use below. To solve for $\hat{c}(\mathbf{x},\lambda_k)$ we use standard finite elements with linear and bilinear interpolation functions in 1-D and 2-D, respectively.

FELT suffer from oscillations (Gibbs phenomenon) arising from non-uniform convergence of the series in (4.7) near discontinuities. This means that the number of terms in (4.7) needed for a given improvement in accuracy tends to become arbitrarily large as one approaches a discontinuity (e.g. [32]). In general, $\hat{c}(\mathbf{x},\lambda_k)$ is an oscillatory function with period Φ that increases with k and depends additionally on $\mathbf{D}$, $\mathbf{v}$, and λ_k. Sudicky [46] showed that for fixed v and λ_k, Φ in 1-D increases with D; for fixed D and λ_k, Φ decreases as v increases. It is easy to show [46] that, under pure advection in a semi-infinite 1-D domain with zero initial concentration and Dirichlet inlet condition, the discretization interval needed for an accurate solution is $\Delta x = 2vt_{\max}/n(2M+1)$ where n is the number of nodes needed to resolve $\hat{c}(\mathbf{x},\lambda_k)$ over a distance Φ and $2M+1$ is the last term in the series (4.7). Therefore, near concentration discontinuities in fixed grid, increasing M in (4.7) leads to improved accuracy up to some limit beyond which $\hat{c}(\mathbf{x},\lambda_k)$ cannot be accurately resolved; to further reduce (though not necessarily eliminate) oscillations, one must increase M and refine the grid simultaneously. Yet when $c(\mathbf{v},t)$ is smooth, a coarse grid produces accurate results with a relatively small value of M [19,46].

4.2 Numerical comparison of ULTIMATE-QUICKEST and FELT

1-D composite initial concentration profile in uniform velocity field

To compare ULTIMATE-QUICKEST with FELT we start by considering the 1-D dimensionless ADE

$$\frac{\partial c}{\partial t}+\frac{\partial c}{\partial x}-\frac{1}{Pe}\frac{\partial^2 c}{\partial x^2}=0, \qquad Pe=\frac{vL}{D}>0, \tag{4.8}$$

on a finite interval $x\in[0,1]$ subject to Dirichlet boundary conditions $c(0,t)=1$, $c(1,t)=0$ and a composite initial concentration profile

$$c(x,0)=\begin{cases} 1 & \text{if } x\in[0.1,0.15] \quad \text{(square)},\\ \cos^2\left(\dfrac{\pi x}{20\Delta x}\right) & \text{if } x\in[0.25,0.35] \quad \text{(squared cosine)},\\ \left(1-\dfrac{(x-0.5)^2}{0.05^2}\right)^{1/2} & \text{if } x\in[0.45,0.55] \quad \text{(semi-ellipse)},\\ 0 & \text{otherwise.}\end{cases} \tag{4.9}$$

Here x is normalized by the length L of the flow domain, $c=C/C_0$ is dimensionless concentration where C_0 is the peak of the initial concentration profile, and $t=v\tau/L$ is

dimensionless time. We use a discretization interval $\Delta x = 0.005$ associated with a grid Peclet number $Pe_g = v\Delta x/D$. For finite Peclet numbers $Pe < \infty$, an analytical solution exists in the form [3]

$$c(x,t) = e^{\frac{Pe}{2}\left(x-\frac{t}{2}\right)} \int_0^1 G(x-x',t)c(x',0)e^{-\frac{Pe}{2}x'}dx' + 0.5\left[erfc(A) + e^{xPe}erfc(B)\right], \qquad (4.10)$$

where G is a Green's function, $A = (x-t)/\sqrt{4t/Pe}$ and $B = (x+t)/\sqrt{4t/Pe}$. For simplicity we adopt the semi-infinite Green's function

$$G(x-x',t-\tau) = \frac{e^{-Pe\frac{(x-x')^2}{4(t-\tau)}} - e^{-Pe\frac{(x+x')^2}{4(t-\tau)}}}{\sqrt{4\pi(t-\tau)/Pe}}, \qquad (4.11)$$

set $\tau = 0$ and evaluate the integral by Gaussian quadrature. To avoid dependence of the numerical solution on the downstream boundary we terminate it before any notable change in concentration would take place close to it.

Preliminary runs of FELT with $c(x,0) = 0$ and $c(0,t) = 1$ have suggested $M = 30$, $\mu = 0$ and $Er = 10^{-8}$. We kept these parameters fixed for all simulations, including those associated with small Pe_g values. We consider two cases:

a) *Infinite Peg (pure advection).* Fig. 1 (left) shows results obtained with ULTIMATE-QUICKEST (ULT) with $Cr = 0.5$ ($\Delta t = 0.0025$) and $Cr = 0.05$ ($\Delta t = 0.00025$) at $t = 0.2$ and 0.4; we note that even though optimal results would be obtained with $Cr = 1$, in variable velocity fields one often has to limit Cr to smaller values, hence these are of practical interest. Fig. 1 (right) shows corresponding results obtained with FELT using the q-d algorithm without (FELT 1) and with (FELT 2) improvement of convergence based on estimates of the continued fraction remainder [14]. FELT 1 and 2 produce oscillatory solutions near discontinuities and appear to have comparable accuracy except at $t = 0.2$ near $x = 0.3$ where FELT 1 produces stronger oscillations. Increasing the value of M to 35 produces a less oscillatory solution for FELT 1 (not shown), similar to that of FELT 2 in Fig. 1; increasing the value of M further reduces accuracy in both FELT versions due to an enhancement of discretization and roundoff errors. Increasing M to 60 while reducing Δx by 1/5 reduces significantly the period of the oscillations and the magnitude of the largest (overshoot) and smallest (undershoot) concentrations at $t = 0.2$ from 2.46 and -0.38 (Fig. 1) to 1.12 and -0.03 (not shown), respectively. Fig. 2 compares the performance of ULT with $Cr = 0.5$ and FELT 2 at $t = 0.2$ and 0.4. ULT generates monotonous results, free of spurious oscillations, though it introduces some smearing of sharp fronts. FELT resolves better the profile of sharp fronts but suffers from spurious oscillations. Since these oscillations depend on the number of terms in (4.7) and the spatial discretization, reducing them requires increasing M and refining the grid to allow better resolution of the complex (periodic) solution in Laplace space.

b) *Pe_g finite (advection-diffusion).* Fig. 3 compares results obtained by the two methods for $Pe_g = 100$ (left) and $Pe_g = 20$ (right), respectively. Here FELT with and without im-

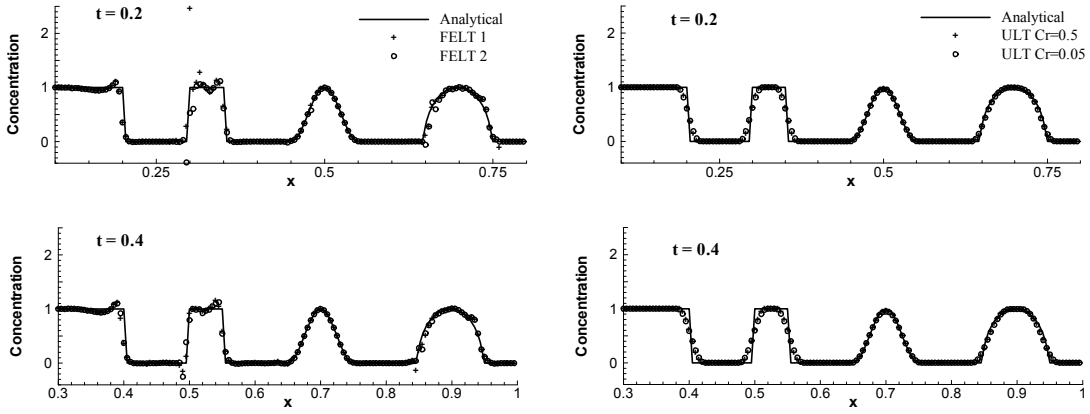

Figure 1: ULTIMATE-QUICKEST (left) and FELT (right) solutions for composite initial concentration and infinite grid Peclet number.

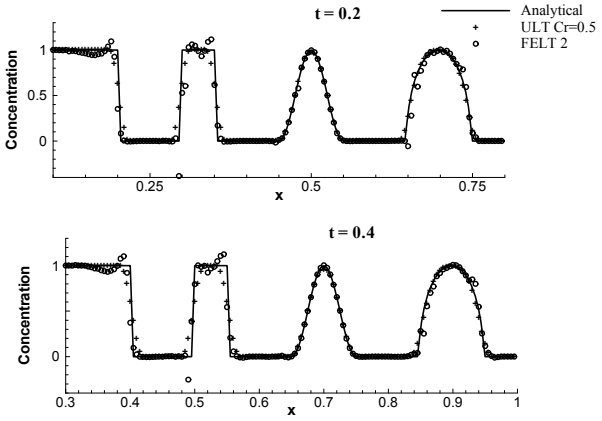

Figure 2: Results of ULT and FELT for composite initial concentration and infinite grid Peclet number.

provement of convergence based on estimates of the continued fraction remainder gave similar results, and we therefore present only those obtained with FELT 2. At $Pe_g = 100$ FELT still suffers from spurious oscillations but to a lesser degree than under pure advection. On the other hand, the FELT solution for $Pe_g = 20$ is free of such oscillations. FELT resolves the squared cosine and semi-elliptic profiles more accurately than does ULT in both cases. The ULT solution is free of oscillations at all times; however, it smears sharp fronts even at the relatively small grid Peclet value of $Pe_g = 20$.

Table 1 compares the solutions in terms of mean squared error (MSE) relative to the analytical solution. Smearing of sharp fronts has an adverse effect on the overall accuracy of ULT, leading to relatively high MSE values. FELT is consistently more accurate except at early time under pure advection where it produces an oscillatory solution. Table 1 also compares execution times. Both schemes were run on a PC with AMD Athlon^{TM} processor. ULT with $Cr = 0.5$ required about four times less central processor (CPU) time than did FELT; however, with $Cr = 0.05$ ULT required almost an order of magnitude more

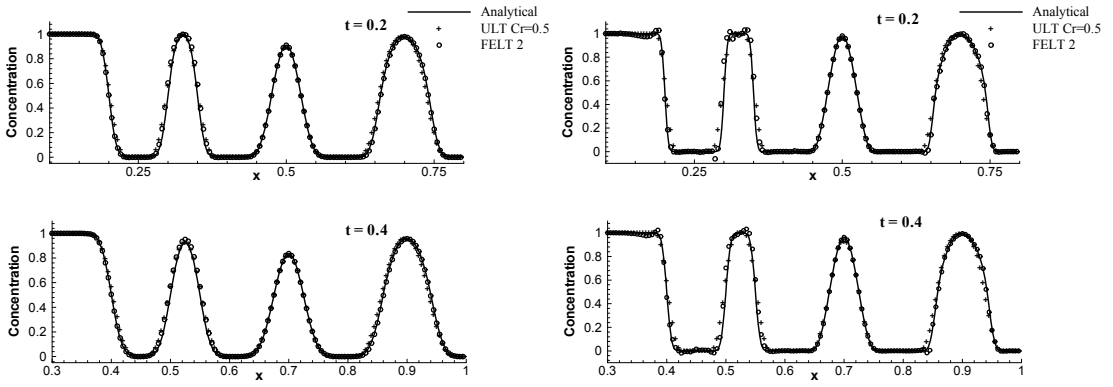

Figure 3: Results of ULT and FELT for composite initial concentration at $Pe_g=100$ (left) and $Pe_g=20$ (right).

CPU time. Table 1 also lists the efficiency index $Eff=[(MSE)(CPUT)]^{-1}$ for $t=0.4$ where $CPUT$ is CPU time: whereas the efficiency index of ULT with $Cr=0.5$ is 2 to 3 times higher than that of FELT, with $Cr=0.05$ it is 3 to 7 times lower.

Table 1: Results for composite initial concentration.

Method	MSE ($\times10-3$) $t=0.2$	$t=0.4$	CPU time (msec)	Eff ($\times10-3$) $t=0.4$
$Pe_g=$ infinite				
ULT, $Cr=0.5$	5.07	6.25	16	10.0
ULT, $Cr=0.05$	6.02	7.40	139	1.0
FELT 1	15.60	4.61	71 (13) [a]	3.1
FELT 2	7.30	5.66	*b*	2.5
$Pe_g=100$				
ULT, $Cr=0.5$	2.09	1.75	16	35.8
ULT, $Cr=0.05$	2.51	2.21	157	2.9
FELT 1	0.82	0.73	71 (12) [a]	19.3
FELT 2	1.22	0.75	*b*	18.8
$Pe_g=20$				
ULT, $Cr=0.5$	0.82	0.62	17	95.6
ULT, $Cr=0.05$	0.90	0.69	156	9.3
FELT 1	0.40	0.27	69 (11) [a]	52.2
FELT 2	0.37	0.27	*b*	52.2

[a] The first number indicates total execution time. The number in parenthesis indicates execution time devoted to finite element solution in Laplace space.
[b] Computed together with FELT 1 as corresponding computational effort is low.

FELT 1 and 2 yield virtually identical results for $Pe_g=5$, 50, 500 at all t when $t_{\max}=1$. The MSE of FELT increases with Pe_g. For a given Pe_g it is relatively small in the time range $0.1t_{\max}<t<1.1t_{\max}$, the lower limit providing a confirmation of similar findings by Gallo et al. [22]. This is expected as at early time the solute has not undergone enough

spreading to smooth out sharp fronts at which truncation errors have the greatest effect. At $t > 1.1t_{\max}$ the solution oscillates at low values of x.

1-D initial delta pulse in uniform velocity field

In our second one-dimensional example we replace the Dirichlet by Neumann boundary conditions $\partial c/\partial x|_{x=0,x=1}=0$ and the initial concentration by $c(x,0)=\delta(x-0.2)$ where δ is the Dirac delta function. In the ULT finite-volume method we interpret the concentration c as a cell-averaged value $c(x,t)=\int_{\Delta x} c^p(x',t)dx'/\Delta x$ where c^p is point concentration and set the initial concentration accordingly to $c(x=0.2,0)=1/\Delta x$. Results for $Pe_g=5$, 10, 20 and $t=0.2$, 0.4 show (Fig. 4 does so for $Pe_g=20$) that FELT performs better than ULT across this range of grid Peclet numbers, becoming comparatively more accurate as Peg increases. At $Pe_g=10$ and 20 ULT suffers from peak clipping and some numerical dispersion. On the other hand, FELT at $Pe_g=20$ suffers from mild oscillations at early time ($t=0.2$) which disappear at late time ($t=0.4$); this is due to the fact that spreading smoothes the profile, allowing a more accurate solution at late time. Table 2 shows that FELT outperforms ULT in terms of the efficiency index Eff in all three cases.

Table 2: Results for initial concentration pulse.

Method	MSE ($\times 10-3$)		CPU time (msec)	Eff ($\times 10-3$)
	$t=0.2$	$t=0.4$		$t=0.4$
$Pe_g=5$				
ULT, $Cr=0.5$	9.09	1.77	20	28.3
ULT, $Cr=0.05$	23.74	5.09	150	1.3
FELT 1	0.36	0.06	160 (100) [a]	100.6
FELT 2	0.36	0.06	*b*	100.6
$Pe_g=10$				
ULT, $Cr=0.5$	148.67	35.94	20	1.4
ULT, $Cr=0.05$	313.08	86.31	160	0.1
FELT 1	2.91	0.42	170 (110) [a]	13.9
FELT 2	3.04	0.42	*b*	13.9
$Pe_g=20$				
ULT, $Cr=0.5$	1185.80	380.83	20	0.1
ULT, $Cr=0.05$	1972.76	713.11	150	0.01
FELT 1	458.75	5.86	170 (110) [a]	1.07
FELT 2	715.83	6.13	*b*	1.02

[a] The first number indicates total execution time. The number in parenthesis indicates execution time devoted to finite element solution in Laplace space.
[b] Computed together with FELT 1 as corresponding computational effort is low.

2-D transport in single realization of random velocity field

Next we consider a rectangular domain with discretization intervals $\Delta x_1=\Delta x_2=0.2$ (Fig. 5). We start by generating a single unconditional realization of a random log hydraulic conductivity field $Y(\mathbf{x})=\ln K(\mathbf{x})$ at element centers using the sequential Gaussian

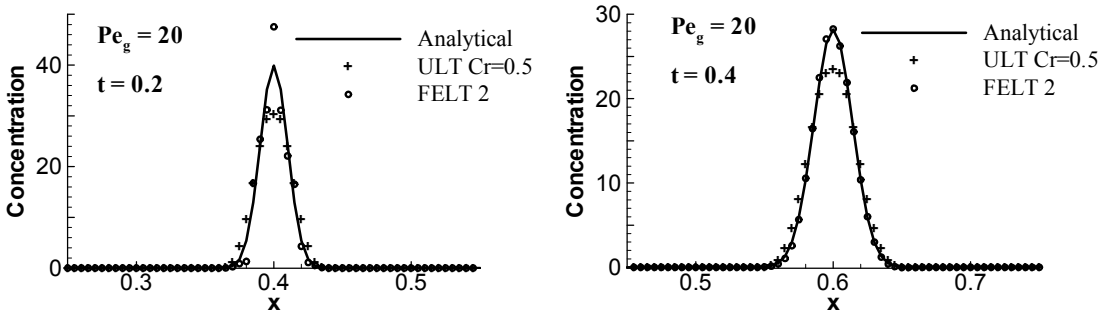

Figure 4: Results of ULT and FELT for initial delta concentration pulse $x=0.2$.

simulation code SGSIM [16]; the point values are then ascribed to the entire element. The generated field has zero mean, variance $\sigma_Y^2=3.0$ (made purposely large to generate large-amplitude spatial fluctuations in Y) and isotropic exponential spatial correlation $C_{YY}(r)=\sigma_Y^2\exp(-r/I_Y)$, where $I_Y=1.0$ is integral scale (made purposely small to generate rapidly fluctuating variations in Y), r being separation distance between any two points in the domain.

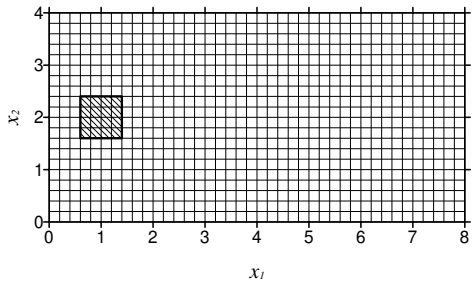

Figure 5: Computational domain with uniform non-zero initial concentration zone (shaded).

We test two solutions of the flow problem. First we use standard Galerkin finite elements with bilinear weight and interpolation functions to compute the steady state distribution of hydraulic heads at all grid nodes subject to prescribed heads of $H=0.8$ at $x_1=0$ and $H=0$ at $x_1=8$ and no-flow across $x_2=0$ and $x_2=4$. Then, using a uniform advective porosity arbitrarily set equal to 1, we compute velocity at the center of each element and ascribe it to the entire element. The resulting velocity field is globally conservative but locally discontinuous and non-conservative which, as will be illustrated, has an adverse affect on the transport solution (e.g. [13, 17]). The velocity field obtained by the standard Galerkin approach can be post-processed to recover local mass conservation [7, 47]. Alternatively we solve the flow problem by cell-centered finite differences and compute velocity at the faces of the elements; the resulting velocity field is locally continuous normal to element faces and locally and globally conservative. By construction ULT requires velocity to be defined at the faces of each element. In the case of FELT, we accommodate

this variable velocity field by using linear interpolation,

$$v_1(\mathbf{x}) \approx v_1(x_1) = w_L(x_1)v_{1L} + w_R(x_1)v_{1R},$$

where $w_L(x_1) = 0.5(1-x_1)$, $w_R(x_1) = 0.5(1+x_1)$ and v_{1L} and v_1R are the velocity values at the left and right face, respectively; v_2 is interpolated in a similar manner in the x_2 direction. Linear interpolation yields discontinuous tangential velocities leading to discontinuities in a velocity-dependent dispersion tensor and affecting mass conservation [31]; however, since in our examples we take local dispersion to be constant, this does not affect our results.

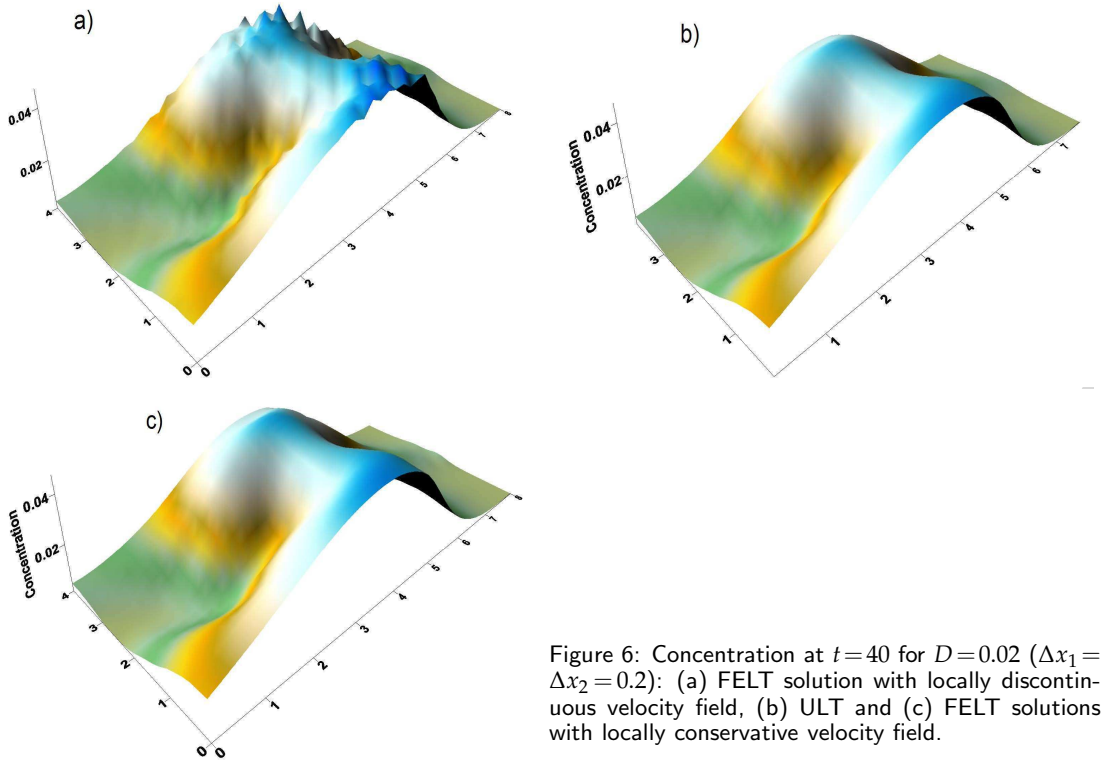

Figure 6: Concentration at $t = 40$ for $D = 0.02$ ($\Delta x_1 = \Delta x_2 = 0.2$): (a) FELT solution with locally discontinuous velocity field, (b) ULT and (c) FELT solutions with locally conservative velocity field.

Transport is computed for three scalar dispersion coefficients $D = 0.02$, 0.002, and 0.0002, corresponding to maximum grid Peclet numbers of approximately 5, 50 and 500 in the x_1 direction and 1.7, 17 and 170 in the x_2 direction, respectively. To compute concentration we set $[\mathbf{v}c - D\nabla c]\cdot\mathbf{n} = 0$ at $x_2 = 0$, $x_2 = 4$ and at $x_1 = 0$, $\partial c/\partial x_1 = 0$ at $x_1 = 8$, $C_0(\mathbf{x}) = 1$ at $0.6 \le x_1 \le 1.4$ and $1.6 \le x_2 \le 2.4$, and $C_0(\mathbf{x}) = 0$ at all other points. The computational grid is the same as that used for flow (Fig. 5). Fig. 6 depicts concentrations at $t = 40$ obtained for $D = 0.02$ using (a) FELT with a locally discontinuous velocity field, and both (b) ULT and (c) FELT with a locally conservative velocity field. Discontinuity of velocity at element faces yields oscillatory concentration values; these unphysical oscillations are

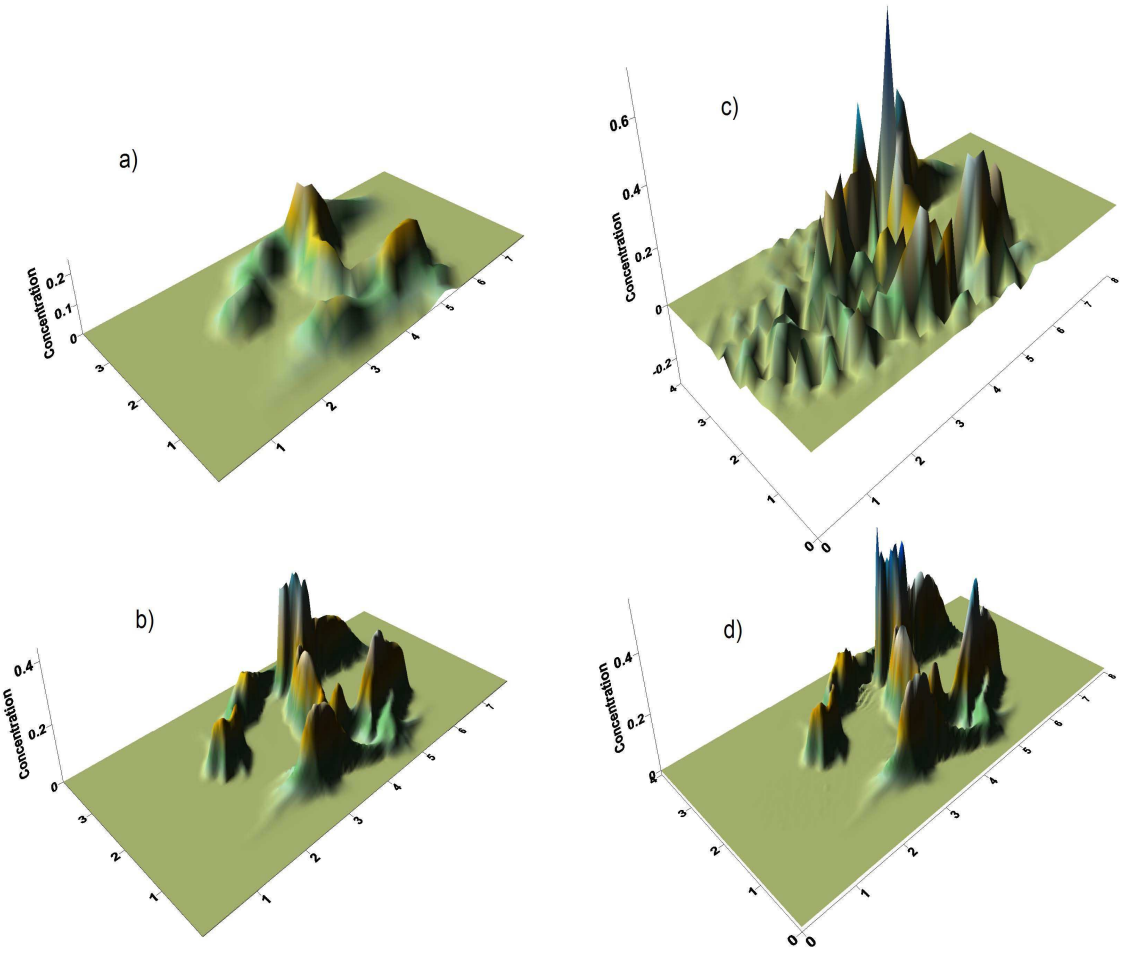

Figure 7: Concentrations at $t=40$ obtained for $D=0.0002$ (maximum grid Peclet number of 500) using (upper left) ULT and (upper right) FELT with $\Delta x_1=\Delta x_2=0.2$ and (lower left) ULT and (lower right) FELT with $\Delta x_1=\Delta x_2=0.05$. The velocity field is locally conservative.

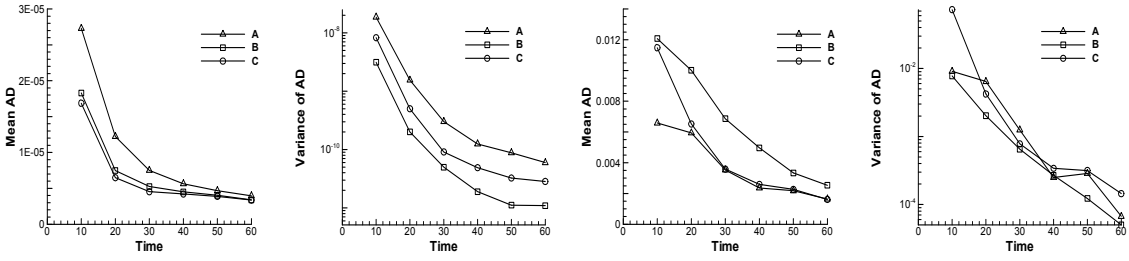

Figure 8: Average and variance of absolute differences (AD) between coarse- and fine-grid solutions for (left) $D=0.02$ and (right) $D=0.0002$ versus time. A = coarse- versus fine-grid ULT solution; B = coarse- versus fine-grid FELT solution; C = ULT versus FELT solutions on fine grid.

absent when the velocity field meets local mass conservation criteria (Fig. 6). Hence in the remainder of this section we present only results obtained using a locally conservative velocity field; however, in a later section we will revisit the locally non-conservative velocity field in the context of Monte Carlo simulations.

Upon decreasing D from 0.02 to 0.002 both ULT and FELT yield accurate solutions when the velocity field is locally conservative (not shown). Fig. 7 depicts ULT and FELT solutions based on a locally conservative velocity field for $D=0.0002$ (increasing the maximum grid Peclet number to 500) for a coarse ($\Delta x_1=\Delta x_2=0.2$) and a fine ($\Delta x_1=\Delta x_2=0.05$) grid. In this case ULT results show a marked sensitivity to grid refinement (Figs. 7(a) and 7(b)) while the coarse-grid FELT solution is plagued by nonphysical negative values of concentration (Fig. 7(c)); these oscillations are greatly reduced when the grid is refined (Fig. 7(d)). FELT oscillations occur in the vicinity of sharp fronts which, in heterogeneous media at high grid Peclet numbers, tend to develop in areas of large velocity contrast.

Fig. 8 shows how the average and variance of the absolute differences AD between coarse- and fine-grid solutions for $D=0.02$ and 0.0002 vary with time. Values of $AD(\mathbf{x}_i,t)=\left|c_{coarse}(\mathbf{x}_i,t)-c_{fine}(\mathbf{x}_i,t)\right|$ are computed at grid nodes in comparing FELT results on coarse and fine grids, at element centers in comparing ULT results on coarse and fine grids, and at element centers in comparing FELT (interpolated by standard finite elements) and ULT results on fine grids. Fig. 8 confirms that, in the case of $D=0.02$, FELT is less sensitive (has smaller average and variance of AD values) to grid refinement than is ULT, suggesting that FELT is more accurate. By the same standard, ULT and FELT are equally accurate in the case of $D=0.002$ (not shown) but ULT is more accurate than FELT in the case of $D=0.0002$ (Fig. 8). In all three cases the variance of AD diminishes rapidly at early time and much more slowly at later time.

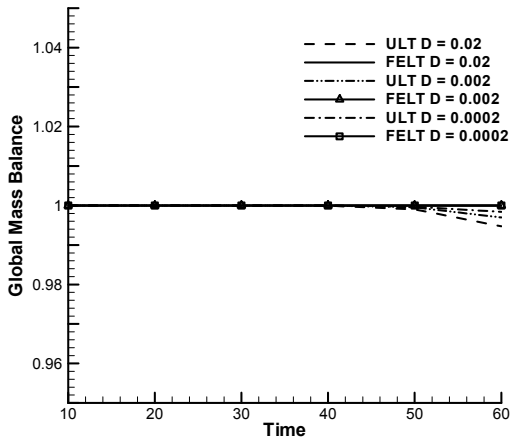

Figure 9: Global mass balance fraction versus time for coarse grid ($\Delta x_1=\Delta x_2=0.2$) ULT and FELT solutions corresponding to various D values.

Global mass balance is expressed by the fraction $MB=[M(t)+BF(t)]/M(t_0)$ where $M(t_0)$ and $M(t)$ stand for total mass in the domain at times t_0 and t, respectively, and

$BF(t)$ is cumulative net solute flux through the boundaries (positive out, negative in). Fig. 9 shows how MB varies with time in the case of coarse grid ($\Delta x_1 = \Delta x_2 = 0.2$) ULT and FELT solutions corresponding to the above three D values. Both methods exhibit excellent global mass balance before the plume reaches the boundary at approximately $t = 50$; for $t > 50$ the mass balance of ULT deteriorates slightly due to insufficient accuracy when computing the time integral representing cumulative mass flux at the boundary; the latter is easier to compute in Laplace space. FELT, despite its oscillatory nature, maintains excellent global mass balance even at high grid Peclet numbers.

Table 3 compares execution times for the above coarse grid solutions. Though FELT required 2 – 2.5 more CPU-time than did ULT, we note that the efficiency of FELT could be improved substantially by taking advantage of its amenability to parallel computation (e.g. [54]), which we have not done in this work.

Table 3: Comparison of execution times for coarse grid solutions ($\Delta x_1 = \Delta x_2 = 0.2$).

Cases	Stability criterion for ULT in consistent units	Execution time in seconds	
		ULT	FELT
$D = 0.02$	0.2991	0.951	2.213
$D = 0.002$		1.022	2.243
$D = 0.0002$		1.032	2.243

Monte Carlo analysis of mean 2-D transport in random velocity field

We end our comparative analysis of ULT and FELT by conducting Monte Carlo (MC) simulations of transport for $\sigma_Y^2 = 0.3$, $D = 0.005$ (case I) and $\sigma_Y^2 = 3$, $D = 0.002$ (case II) on the rectangular domain depicted in Fig. 5. We adopt the previous procedure to generate numerous (1000 in case I and 3000 in case II) unconditional realizations of $Y(\mathbf{x})$, corresponding realizations of velocity and time-varying concentration fields. In computing each realization of the velocity field we employ both approaches described in the previous section, namely locally discontinuous velocities from standard Galerkin interpolation and locally conservative velocities from a finite difference solution. Comparing these two approaches to obtain the velocity field is of interest because previous stochastic analysis of flow and transport [24, 25, 37, 38, 54] have relied on the first approach. Fig. 10 depicts mean concentration at $t = 40$ for cases I and II when the underlying velocity field is locally conservative; both methods yield similar mean concentrations with minor differences. We thus proceed to compare FELT results when the velocity field is not locally conservative. Fig. 11 shows that oscillations present when the velocity field is not locally conservative (Fig. 6(a)) are smoothed when one averages many realizations (dashed in Fig. 11). For small values of σ_Y^2 the mean and variance of concentration obtained with locally nonconservative velocities are reasonably accurate, though they deteriorate as σ_Y^2 increases. Fig. 12 shows the same to hold for mean solute flux. This confirms the accuracy of results presented elsewhere [37, 38] for $\sigma_Y^2 \leq 0.3$, summarized in the next section.

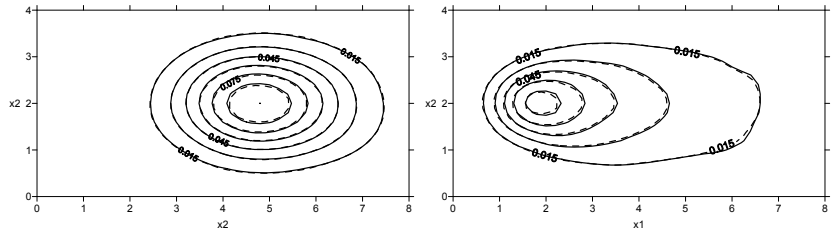

Figure 10: Mean concentration at $t=40$ obtained using ULT (dashed) and FELT (solid) in (left) case I ($\sigma_Y^2=0.3$, $D=0.005$, 1000 Monte Carlo runs) and (right) case II ($\sigma_Y^2=3$, $D=0.002$, 3000 Monte Carlo runs).

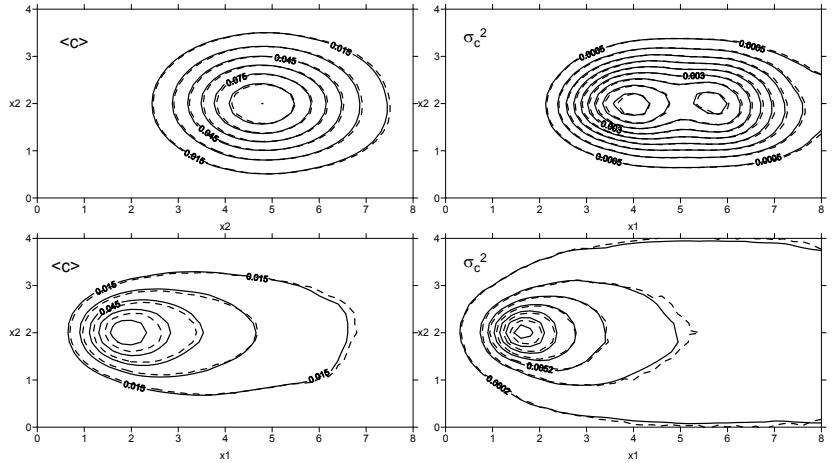

Figure 11: Mean (left) and variance (right) of concentration at $t=40$ obtained using FELT when the velocity field is locally conservative (solid) and locally nonconservative (dashed) in case I ($\sigma_Y^2=0.3$, $D=0.005$, 1000 Monte Carlo runs, top) and case II ($\sigma_Y^2=3$, $D=0.002$, 3000 Monte Carlo runs, bottom).

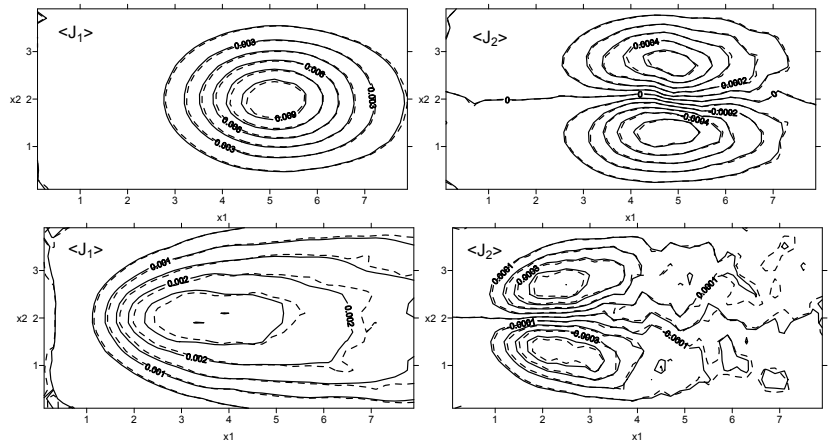

Figure 12: Mean solute flux $t=40$ obtained using FELT when the velocity field is locally conservative (solid) and locally nonconservative (dashed) in case I ($\sigma_Y^2=0.3$, $D=0.005$, 1000 Monte Carlo runs, top) and case II ($\sigma_Y^2=3$, $D=0.002$, 3000 Monte Carlo runs, bottom).

Table 4: Comparison of execution times for coarse grid solutions ($\Delta x_1 = \Delta x_2 = 0.2$).

Case	σ_Y^2	Execution time (h:min:s)	
		FELT	ULT
I (1000 MC runs)	0.3	1:23:45	22:51
II (3000 MC runs)	3.0	4:13:50	7:47:16

Table 4 compares execution times for MC simulations using the two methods. In case I ULT required roughly one fourth the CPU time needed for FELT to attain comparable accuracy; in case II this difference was reduced to about one half. The increase in execution time was caused by a need to reduce ULT time step size in order to comply with the Courant-Friedrich-Lewy condition when higher values of σ_Y^2 produced larger contrasts in velocity.

We conclude by observing that whereas the plume of mean concentrations is symmetric in case I, it is non-symmetric in case II (Fig. 10). The lack of symmetry is due to our imposition of zero solute mass flux across the upstream boundary, which prevents spread (macrodispersion) of the mean plume across it. We emphasize that this spread does not represent physical dispersion but loss of information about the unknown true (random) concentration, as explained by Morales-Casique et al. [37,38].

5 Conditional nonlocal and localized FELT solution compared with Monte Carlo simulations

We review below selected computational results of those previously reported by Morales-Casique et al. [38].

Computational domain and random velocity field

Morales-Casique et al. [38] consider advective-dispersive transport in a rectangular domain of length $8I_Y$ and width $4I_Y$, discretized into square elements of size $\Delta x_1 = \Delta x_2 = 0.2I_Y$ (Fig. 13); all variables are expressed in arbitrary consistent units. Though the moment equations are distribution-free, for purposes of Monte Carlo simulation they take Y to be multivariate Gaussian with mean zero, variance σ_Y^2 and isotropic exponential spatial correlation function $C_{YY}(r) = \sigma_Y^2 \exp(-r/I_y)$ where r is separation distance. The authors generate a single unconditional realization of Y at element centers using the sequential Gaussian simulation code SGSIM [16] and ascribing it to the entire element. They then "measure Y exactly" at 18 conditioning points shown by solid squares in Fig. 13, use SGSIM in the above manner to generate numerous realizations of Y conditioned on these "measurements", and evaluate the corresponding first and second sample moments of the generated conditional Y fields.

To generate corresponding statistics of time-independent advective velocity, Morales-Casique et al. [38] use conditional Monte Carlo simulations and the recursive finite ele-

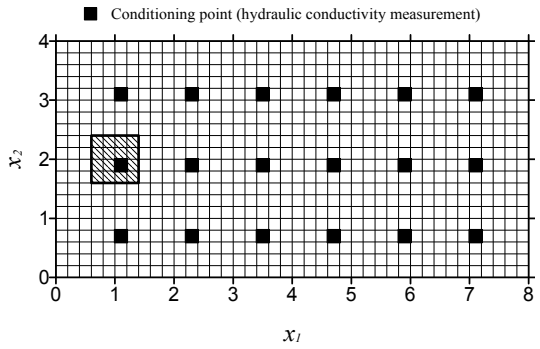

Figure 13: Computational domain and grid, conditioning points and location of initial non-zero concentration (shaded).

ment moment algorithm of Guadagnini and Neuman [24, 25], both on the above grid. In the case of Monte Carlo simulations, they use standard finite elements to solve a deterministic steady state flow problem for each conditional realization of Y and compute first and second sample moments of the corresponding advective velocity realizations. The resulting velocity in each realization is constant in each element and thus not locally conservative; however, we are interested in moments of these realizations which, as shown in the previous section, are reasonably accurate for small values of σ_Y^2. The moment algorithm uses first and second conditional moments of Y to compute directly first and second conditional velocity moments to second order in σ_Y. In both cases advective porosity is set (for simplicity) equal to 1, head is set equal to $H=0.8$ at $x_1=0$ and $H=0$ at $x_1=8$, and no-flow conditions are imposed across $x_2=0$ and $x_2=4$. For $\langle Y\rangle_c=0$, $\sigma_Y^2=0.3$ and $I_Y=1$, 3000 Monte Carlo simulations and the recursive algorithm yield comparable first and second conditional velocity moments. The authors found that for $\sigma_Y^2=0.3$ the unconditional longitudinal velocity v_1 follows closely a lognormal distribution. Unconditional transverse velocity decays more slowly than a Gaussian distribution at the tails, most likely due to the effect of boundaries. Conditioning brings the distributions of both velocity components closer to Gaussian.

Transport computations

To compute transport variables Morales-Casique et al. [38] set $\mathbf{D}_d=D_d\mathbf{I}$ where $\mathbf{I}$ is the identity tensor, $[\mathbf{v}c-D_d\nabla c]\cdot\mathbf{n}=0$ at $x_2=0$ and $x_2=4$, $[\mathbf{v}c-D_d\nabla c]\cdot\mathbf{n}=0$ at $x_1=0$, $\partial c/\partial x_1=0$ at $x_1=8$, $C_0(\mathbf{x})=1$ at $0.6\le x_1\le 1.4$ and $1.6\le x_2\le 2.4$, and $C_0(\mathbf{x})=0$ at all other points. They present results in terms of a Peclet number $Pe=u_1I_Y/D_d$ where $u_1=0.1$ is the (theoretical) unconditional mean velocity parallel to x_1, and a grid Peclet number $Pe_g=u_1\Delta x_1/D_d$. All results, including Monte Carlo simulations, are obtained using FELT. For the recursive and iterative algorithms the authors use ensemble velocity moments obtained using the flow moment algorithm of Guadagnini and Neuman [24, 25]. They conduct Monte Carlo simulations of transport by solving the stochastic transport equations (2.1)-(2.6), for each conditional realization of velocity, using the above grid.

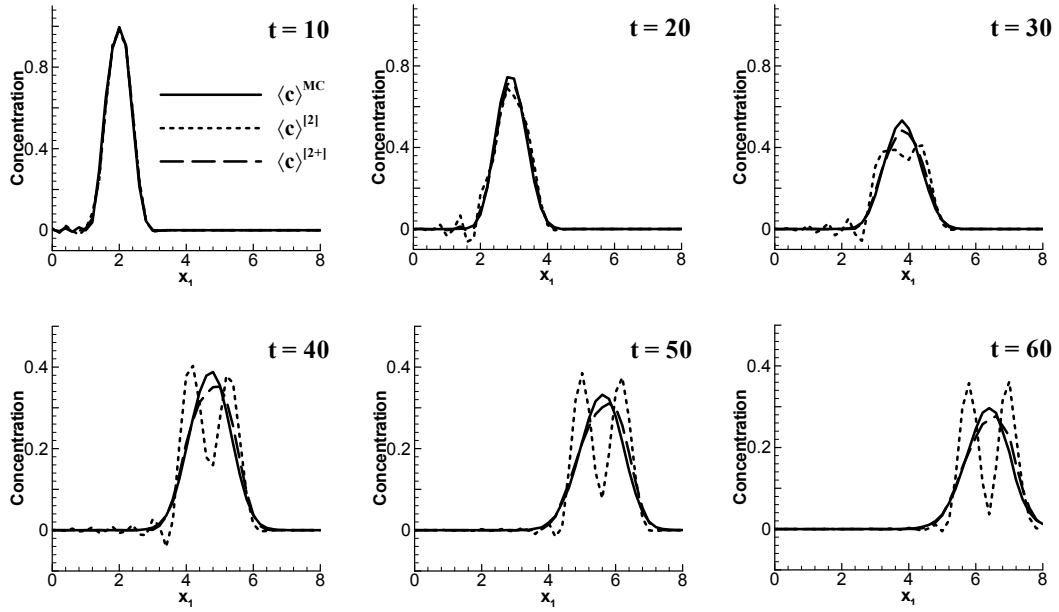

Figure 14: Conditional mean concentration profile at $x_2=2.0$ and $t=10$, 20, 30, 40, 50, 60 for $\sigma_Y^2=0.3$, $I_Y=1$, $D_d=0.001$, $Pe=100$ and $Pe_g=20$ based on 3000 Monte Carlo simulations $\langle c\rangle^{MC}$, second-order recursive $\langle c\rangle^{[2]}$ and iterative $\langle c\rangle^{[2+]}$ nonlocal moment equations.

Fig. 14 depicts conditional mean concentration profile at $x_2=2.0$ and $t=10$, 20 30, 40, 50, 60 for $\sigma_Y^2=0.3$, $I_Y=1$, $D_d=0.001$, $Pe=100$ and $Pe_g=20$ based on 3000 Monte Carlo simulations $\langle c\rangle^{MC}$, second-order recursive $\langle c\rangle^{[2]}$ and iterative $\langle c\rangle^{[2+]}$ nonlocal moment equations. There is a pronounced bimodal behavior of the recursive mean concentration. Neither the Monte Carlo nor the iterative mean concentration, which are in close agreement with each other, exhibit such bimodality. These results and 1D simulations (not shown) indicate that second and third-order perturbation terms are oscillatory, that this oscillatory behavior increases with time, and that many terms in a standard perturbation series may be needed for convergence. This oscillatory behavior is not caused by the mean velocity being constant in each element (and thus locally nonconservative). This is evidenced by (a) the smooth and nonoscillatory nature of the zero-order concentration $\langle c\rangle^{(0)}$ (Fig. 9 in [38]) and (b) the frequency of the oscillations in the second-order correction $\langle c\rangle^{(2)}$ (Fig. 9 in [38]) being much larger than that due to discontinuities in the velocity field (see Fig. 6(a)). The iterative solution provides more accurate results than does standard perturbation because it approximates the dispersive flux more closely and could be improved further by accounting for velocity moments of order higher than two.

Fig. 15 shows conditional mean concentration profiles at $x_2=2$ and $t=10$, 50 for the above parameters based on Monte Carlo simulations compared with iterative nonlocal and space-localized moment solutions. The space-localized solution is seen to be inferior, exhibiting spurious oscillations (undershoot) at early time while underestimating

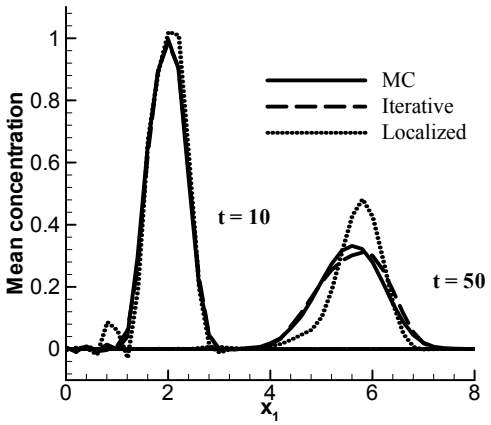

Figure 15: Conditional mean concentration profiles at $x_2=2$ and $t=10$, 50 for $\sigma_Y^2=0.3$, $I_Y=1$, $D_d=0.001$, $Pe=100$ and $Pe_g=20$ based on 3000 Monte Carlo simulations compared with iterative nonlocal and space-localized moment solutions.

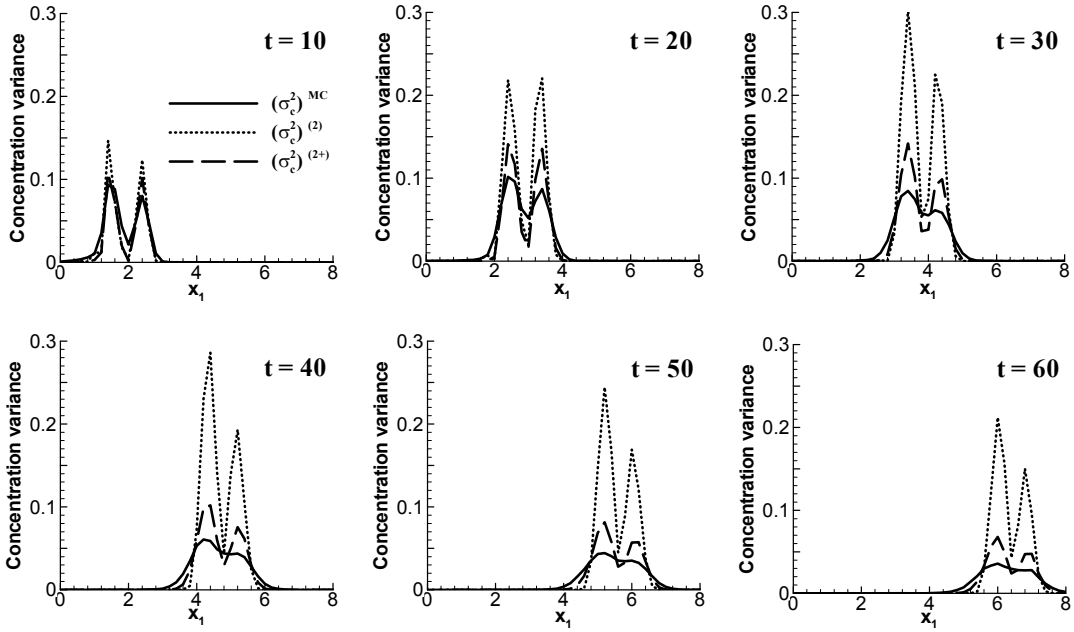

Figure 16: Conditional concentration variance profile at $x_2=2$ and $t=10$, 20, 30, 40, 50, 60 for $\sigma_Y^2=0.3$, $I_Y=1$, $D_d=0.001$, $Pe=100$ and $Pe_g=20$ based on 3000 Monte Carlo simulations $\langle c\rangle^{MC}$, second-order recursive $\langle c\rangle^{[2]}$ and iterative $\langle c\rangle^{[2+]}$ nonlocal moment equations.

dispersion, overestimating the peak and causing a downstream shift in the peak and the receding limb of the mean concentration profile.

Fig. 16 depicts profiles of conditional concentration variance about the mean values in Fig. 14 based on 3000 Monte Carlo simulations $(\sigma_c^2)^{MC}$, second-order recursive $(\sigma_c^2)^{(2)}$ and iterative $(\sigma_c^2)^{(2+)}$ nonlocal moment equations. Although both moment solutions deteriorate with time and overestimate the peak variance, $(\sigma_c^2)^{(2+)}$ is much closer to $(\sigma_c^2)^{MC}$

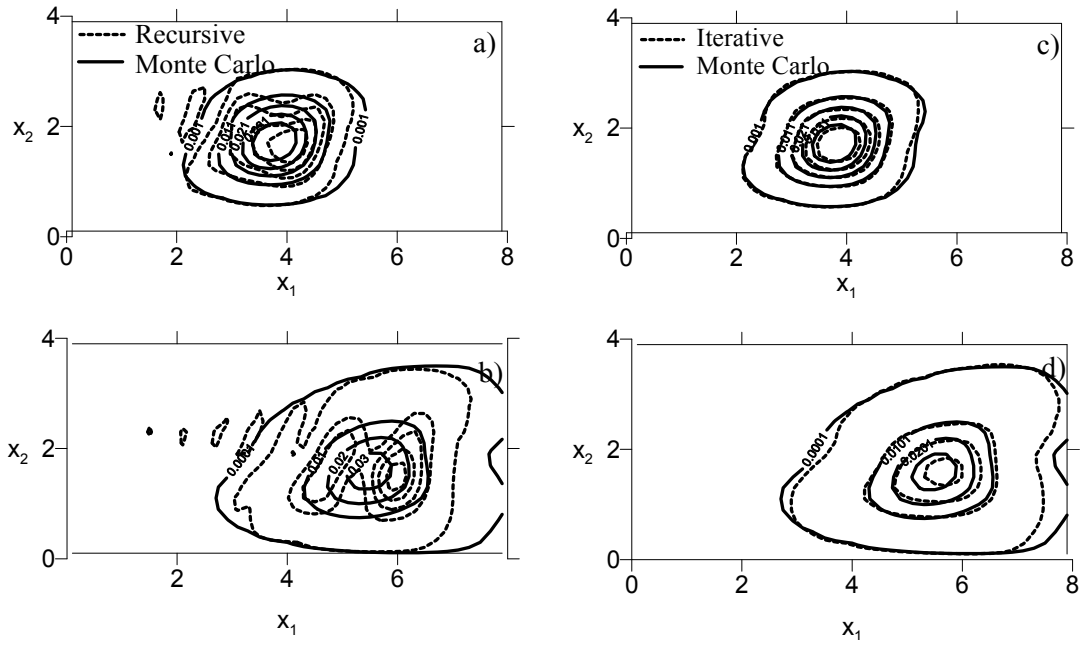

Figure 17: Longitudinal component (parallel to x_1) of conditional mean solute mass flux contours at $t=30$ and 50 for $\sigma_Y^2=0.3$, $I_Y=1$, $D_d=0.001$, $Pe=100$ and $Pe_g=20$ based on 3000 Monte Carlo simulations compared with second-order recursive (a - b) and iterative (c - d) nonlocal moment solutions.

than $(\sigma_c^2)^{(2)}$ and thus considerably more accurate.

Fig. 17 depicts contours of the longitudinal component (parallel to x_1) of conditional mean solute mass flux at $t=30$, 50 for the above parameters based on 3000 Monte Carlo simulations compared with second-order recursive and iterative nonlocal moment solutions $\langle J_1\rangle_c^{[2]}$ and $\langle J_1\rangle_c^{[2+]}$. Whereas the iterative solution is quite accurate, the same is not true about the recursive solution which exhibits some unwarranted bimodality due to the bimodal behavior of $\langle c\rangle_c^{[2]}$ and inaccurate resolution of the dispersive flux.

Execution time

Morales-Casique et al. [38] conducted their analysis on a HP/Compaq Alpha supercomputer at the University of Arizona in Tucson. Since their emphasis was on accuracy rather than computational efficiency, they have not made an attempt to optimize their codes or take advantage of parallelization. For their parameters 3000 conditional Monte Carlo runs (of transport only) required 16,558 seconds to execute, in comparison to 226 seconds for the non-iterative second-order recursive moment approach and 1,500 for 15 iterations of the higher-accuracy iterative moment approach. In other words, conditional Monte Carlo simulation required over 73 times more computer time than the second-order recursive moment solution and 11 times more than the iterative solution.

6 Conclusions

Our analysis leads to the following conclusions:

1. It is possible and computationally feasible to obtain accurate, unbiased predictions of nonreactive solute transport in bounded randomly heterogeneous porous media, and to assess the corresponding predictive uncertainty, without Monte Carlo simulation. We have shown results for time-independent velocity in two dimensions obtained with an iterative finite element algorithm based on Laplace-transformed conditional moment equations and numerical inversion of the results back into the time domain, FELT.

2. We compared FELT numerically with a high-accuracy ULTIMATE-QUICKEST (ULT) algorithm coupled with an alternating split operator approach. In the relatively simple 1-D case of a composite concentration profile propagating at uniform velocity, both methods do an excellent job in controlling (FELT) or eliminating (ULT) oscillations even under pure advection; however, FELT becomes more accurate as the grid Peclet number diminishes. In the corresponding case of an instantaneous point source, FELT is more accurate than ULT for grid Peclet numbers as high as 20, the latter exhibiting peak clipping and some numerical smearing. In the more complex 2-D case of transport in a randomly varying velocity field arising from random medium heterogeneity, FELT at relatively small (≤ 5) grid Peclet numbers is less sensitive to grid refinement than is ULT and is correspondingly more accurate. ULT and FELT are equally accurate at intermediate grid Peclet numbers (≤ 50) but ULT is more accurate than FELT at large grid Peclet numbers (≤ 500) , the later producing negative concentrations that can be reduced through grid refinement.

3. Our results illustrate the importance of rendering velocity locally conservative; not doing so leads to unphysical oscillations in the transport solution near discontinuities in velocity. In mildly heterogeneous random media (natural log hydraulic conductivity variance $\sigma_Y^2 = 0.3$) averaging random oscillatory solutions corresponding to nonconservative velocities has the effect of smoothing such oscillations. Consequently, the mean and variance of concentration and mean solute flux are not sensitive to how conservative the local velocity may or may not be. However the accuracy of results obtained with nonconservative velocities deteriorates as σ_Y^2 increases beyond 0.3.

4. Conditional results compare well with Monte Carlo simulations for $\sigma_Y^2 = 0.3$ (variance of natural log hydraulic conductivity Y) and Peclet number $Pe = 100$ (defined in terms of mean velocity and the integral scale of Y). In the unconditional case this is true only for $Pe = 10$. As σ_Y^2, Pe and time increase the quality of our iterative moment solution deteriorates. We attribute this to our disregard of the space-time correlation function $\langle c'\mathbf{v}'\mathbf{v}'\rangle_c$ in the computation of dispersive flux. To leading order, this function depends on third velocity moments, which have been shown to gain significance with increasing σ_Y^2, Pe and time but loose significance with conditioning. This appears to be linked to the fact that both longitudinal and transverse velocities depart from Gaussian distribution as σ_Y increases and the level of conditioning decreases.

5. Second-order recursive nonlocal and space-localized results are considerably less

accurate than those obtained with the iterative nonlocal algorithm.

6. In runs conducted on a relatively small grid without optimizing any of the algorithms and without parallelization, the moment solutions required considerably less computer time than did Monte Carlo simulations.

Acknowledgments

This work was supported in part by NSF/ITR Grant EAR-0110289 and through a scholarship granted to the lead author by CONACYT of Mexico. We thank an anonymous reviewer for insightful comments and suggestions that helped improve our paper.

References

[1] M. Al-Lawatia, R. C. Sharpley and H. Wang, Second-order characteristic methods for advection-diffusion equations and comparison to other schemes, Adv. Water Resour., 22(7) (1999), 741-768.
[2] R. P. Batycky, M. J. Blunt and M. R. Thiele, A 3D field scale streamline simulator, SPE Reservoir Engineering, 12 (1997), 246-254.
[3] J. V. Beck, K. D. Cole, A. Haji-Sheikh and B. Litkouhi, Heat Conduction Using Green'S Functions, Series in Computational Methods in Mechanics and Thermal Sciences, Hemisphere Publishing Corporation, London, 1992.
[4] J. Boris and D. Book, Flux-corrected transport I, SHASTA, a fluid transport algorithm that works, J. Comput. Phys., 11 (1973), 38-69.
[5] M. A. Celia, T. A. Russell, I. Herrera and R. E. Ewing, An Eulerian-Lagrangian localized adjoint method for the advection-diffusion equation, Adv. Water Resour., 13 (1990), 187-206.
[6] P. Collela, P. R. Woodward, The piecewise parabolic method (PPM) for gas-dynamical simulations, J. Comput. Phys., 54 (1984), 174-201.
[7] Cordes and W. Kinzelbach, Continuous groundwater velocity fields and path lines in linear, bilinear, and trilinear finite elements, Water Resour. Res., 28 (1992), 2903-2911.
[8] R. A. Cox and T. Nishikawa, A new total variation diminishing scheme for the solution of advective-dominant solute transport, Water Resour. Res., 27 (1991), 2645-2654.
[9] K. S. Crump, Numerical inversion of Laplace transforms using a Fourier series approximation, J. Assoc. Comput. Mach., 23 (1976), 89-96.
[10] J. H. Cushman and T. R. Ginn, Nonlocal dispersion in media with continuously evolving scales of heterogeneity, Transport Porous Med., 13(1) (1993), 123-38.
[11] G. Dagan and S.P. Neuman (editors), Subsurface Flow and Transport: A Stochastic Approach, Cambridge University Press, 1997.
[12] A. Datta-Gupta and M. J. King, A semianalytical approach to tracer flow modeling in heterogeneous permeable media, Adv. Water Resour., 18 (1995), 9-24.
[13] C. Dawson, Conservative, shock-capturing transport methods with nonconservative velocity approximations, Computational Geosciences, 3 (1999), 205-227.
[14] F. R. De Hoog, J. H. Knight and A. N. Stokes, An improved method for numerical inversion of Laplace transforms, SIAM J. Stat. Comput., 3(3) (1982), 357-366.
[15] F.-W. Deng, J. H. Cushman and J. W. Delleur, A fast Fourier transform stochastic analysis of the contaminant transport problem, Water Resour. Res., 29(9) (1993), 3241-3247.

[16] C. V. Deutsch and A. G. Journel, GSLIB Geostatistical Software Library And User's Guide, 2nd ed, Oxford University Press, New York, 1998.
[17] L. J. Durlofsky, Accuracy of mixed and control volume finite element approximations to Darcy velocity and related quantities, Water Resources Research, 30 (1994), 965-973.
[18] R. E. Ewing and H. Wang, A summary of numerical methods for time-dependent advection-dominated partial differential equations, J. Comput. Appl. Math., 128 (2001), 423-445.
[19] D. A. Farrell, A. D. Woodbury and E. A. Sudicky, Numerical modeling of mass transport in hydrogelogic environments: performance comparison of the Laplace Transform Galerkin and Arnoldi modal reduction schemes, Adv. Water Resour., 21 (1996), 217-235.
[20] M. W. Farthing and C. T. Miller, A comparison of high-resolution, finite-volume, adaptive-stencil schemes for simulating advective-dispersive transport, Adv. Water Resour., 24 (2001), 29-48.
[21] C. A. J. Fletcher, Computational Techniques For Fluid Dynamics 1, Fundamentals and General Techniques, 2nd ed., Springer-Verlag, Berlin, 1991.
[22] C. Gallo, C. Paniconi and G. Gambolati, Comparison of solution approaches for the two-domain model of nonequilibrium transport in porous media, Adv. Water Resour., 19 (1996), 241-253.
[23] A. Guadagnini and S. P. Neuman, Recursive conditional moment equations for advective transport in randomly heterogeneous velocity fields, Transport Porous Med., 42(1-2) (2001), 37-67.
[24] A. Guadagnini and S. P. Neuman, Nonlocal and localized analyses of conditional mean steady state flow in bounded, randomly nonuniform domains. 1. Theory and computational approach, Water Resour. Res., 35(10) (1999), 2999-3018.
[25] A. Guadagnini and S. P. Neuman, Nonlocal and localized analyses of conditional mean steady state flow in bounded, randomly nonuniform domains. 2. Computational examples, Water Resour. Res., 35(10) (1999), 3019-3039.
[26] A. Harten and S. Osher, Uniformly high order accurate essentially nonoscillatory schemes I, SIAM J. Numer. Anal., 24 (1987), 279-309.
[27] A. Harten, B. Engquist, S. Osher and S. Chakravarthy, Uniformly high order accurate essentially nonoscillatory schemes III, J. Comput. Phys., 71 (1987), 231-303.
[28] A. F. Hernandez, S. P. Neuman, A. Guadagnini and J. Carrera, Conditioning mean steady state flow on hydraulic head and conductivity through geostatistical inversion, Stoch. Env. Res. Risk. Assess., 17(5) (2003), 329-38.
[29] I. Herrera, R. E. Ewing, M. A. Celia and T. A. Russell, Eulerian-Lagrangian localized adjoint method: The theoretical framework, Numer. Meth. Partial Diff. Eq., 9 (1993), 431-457.
[30] D. L. Koch and J. F. Brady, Anomalous diffusion in heterogeneous porous media, Phys. Fluids, 31 (1988), 965-973.
[31] E. M. LaBolle, G. E. Fogg and A. F. B. Thompson, Random-walk simulation of transport in heterogeneous porous media: Local mass-conservation problem and implementation methods, Water Resources Research, 32 (1996), 583-593.
[32] C. Lanczos, Discourse On Fourier Series, Hafner Publishing Company, New York, 1966.
[33] B. P. Leonard, The ULTIMATE conservative difference scheme applied to unsteady one-dimensional advection, Comp. Meth. Appl. Mech. Eng., 88 (1991), 17-74.
[34] B. P. Leonard and H. S. Niknafs, Cost-effective accurate coarse-grid method for highly convective multidimensional unsteady flows, in: NASA Conference Publication 3078: Computational Fluid Dynamics Symposium on Aeropropulsion, Washington, DC, 1990.
[35] R. J. LeVeque, Numerical Methods for Conservation Laws, Birkhauser-Verlag, 1992.

[36] R. LeVeque and J. Oliger, Numerical methods based on additive splittings for hyperbolic partial differential equations, Math. Comp., 40 (1983), 469-497.
[37] E. Morales-Casique, S. P. Neuman and A. Guadagnini, Nonlocal and localized analyses of nonreactive solute transport in bounded randomly heterogeneous porous media: Theoretical framework, Adv. Water Res., 29 (2006), 1238-1255.
[38] E. Morales-Casique, S. P. Neuman and A. Guadagnini, Nonlocal and localized analyses of nonreactive solute transport in bounded randomly heterogeneous porous media: Computational analysis, Adv. Water Res., 29 (2006), 1399-1418.
[39] S. P. Neuman, Eulerian-Lagrangian theory of transport in spacetime nonstationary velocity fields: exact nonlocal formalism by conditional moments and weak approximation, Water Resour. Res., 29(3) (1993), 633-645.
[40] S. P. Neuman and S. Orr, Prediction of steady state flow in nonuniform geologic media by conditional moments: exact nonlocal formalism, effective conductivities, and weak approximation, Water Resour. Res., 29(2) (1993), 341-364.
[41] S. P. Neuman, D. M. Tartakovsky, T. C. Wallstrom and C. L. Winter, Correction to "Prediction of steady state flow in nonuniform geologic media by conditional moments: exact nonlocal formalism, effective conductivities, and weak approximation" by S.P. Neuman and S. Orr, Water Resour. Res., 32(5) (1996), 1479-1480.
[42] B. Nour-Omid, W. S. Dunbar and A. D. Woodbury, Lanczos and Amoldi methods for solution of convection-diffusion equations, Comput. Methods Appl. Mech. Eng., 88 (1991), 75-95.
[43] P. L. Roe, Some contributions to the modeling of discontinuous flows, Lect. Notes Appl. Math., 22 (1985), 163-193.
[44] Y. Rubin, Applied Stochastic Hydrogeology, Oxford University Press, 2003.
[45] G. Strang, On the construction and comparison of difference schemes, SIAM J. Numer. Anal., 5(3) (1968), 506-517.
[46] E. A. Sudicky, The Laplace transform Galerkin technique: A time continuous finite element theory an application to transport in groundwater, Water Resour. Res., 25(8) (1989),1833-1846.
[47] S. Sun and M. F. Wheeler, Projections of velocity data for the compatibility with transport, Comput. Methods Appl. Mech. Engrg., 195 (2006), 653-673.
[48] D. M. Tartakovsky and S. P. Neuman, Transient flow in bounded randomly heterogeneous domains. 1. Exact conditional moment equations and recursive approximations, Water Resour. Res., 34(1) (1998), 1-12.
[49] D. M. Tartakovsky and S. P. Neuman, Transient effective hydraulic conductivities under slowly and rapidly varying mean gradients in bounded three-dimensional random media, Water Resour. Res., 34(1) (1998), 21-32.
[50] D. M. Tartakovsky and S. P. Neuman, Extension of transient flow in bounded randomly heterogeneous domains. 1. Exact conditional moment equations and recursive approximations, Water Resour. Res., 35(6) (1999), 1921-1925.
[51] E. F. Toro, Riemann Solvers And Numerical Methods For Fluid Dynamics, Springer, London, 1998.
[52] B. van Leer, Towards the ultimate conservative difference scheme V. A second order sequel to Godunov's method, J. Comput. Phys., 32 (1979), 101-136.
[53] A. D. Woodbury, W. S. Dunbar and B. Nour-Omid, Application of the Arnoldi algorithm to the solution of the advection-dispersion equation, Water Resour. Res., 26(10) (1990), 2579-2590.

[54] M. Ye, S. P. Neuman, A. Guadagnini and D. M. Tartakovsky, Nonlocal and localized analyses of conditional mean transient flow in bounded, randomly heterogeneous porous media, Water Resour. Res., 40(5) (2004), W05104.
[55] D. Zhang, Stochastic Methods for Flow in Porous Media: Coping With Uncertainties, Elsevier, 2002.
[56] D. Zhang and S. P. Neuman, Effect of local dispersion on solute transport in randomly heterogeneous media. Water Resour. Res., 32(9) (1996), 2715-2723.
[57] C. Zheng and P. P. Wang, MGO: A Modular Groundwater Optimizer Incorporating MODFLOW and MT3DMS; Documentation and User's Guide, University of Alabama and Groundwater Systems Research Ltd., 2003.